Low-Complexity Equalization of Orthogonal Signal-Division Multiplexing in Doubly-Selective Channels

Han, Jing; Zhang, Lingling; Zhang, Qunfei; Leus, Geert

DOI
10.1109/TSP.2018.2887191

Publication date
2019

Document Version
Final published version

Published in
IEEE Transactions on Signal Processing

Citation (APA)
Han, J., Zhang, L., Zhang, Q., & Leus, G. (2019). Low-Complexity Equalization of Orthogonal Signal-Division Multiplexing in Doubly-Selective Channels. *IEEE Transactions on Signal Processing*, *67*(4), 915-929. Article 8579192. https://doi.org/10.1109/TSP.2018.2887191

Low-Complexity Equalization of Orthogonal Signal-Division Multiplexing in Doubly-Selective Channels

Jing Han, *Member, IEEE*, Lingling Zhang, *Member, IEEE*, Qunfei Zhang, *Member, IEEE*, and Geert Leus, *Fellow, IEEE*

***Abstract*—Orthogonal signal-division multiplexing (OSDM) is a generalized modulation scheme to bridge the gap between orthogonal frequency-division multiplexing (OFDM) and single-carrier frequency-domain equalization. It allows significantly more flexibility in system design; however, over doubly-selective channels, it suffers from a special signal distortion structure, namely inter-vector interference, which is analogous to inter-carrier interference in conventional OFDM. To analyze its effect, in this paper, the complex exponential basis expansion model (CE-BEM) is used to approximate the doubly-selective channel. We show that the composite channel matrix of OSDM systems is cyclically block banded in this case, and the blocks in its main band can be further diagonalized. By exploiting this unique matrix structure, low-complexity block and serial OSDM equalization algorithms are then proposed. These two equalization algorithms are based on block LDL^H factorization and block iterative matrix inversion, respectively, both of which are implemented in a transformed domain to avoid direct inversion of large matrices. In addition, a CE-BEM channel estimation method is designed for OSDM systems, which uses frequency-shifted Chu sequences as pilots to ease the computation. Numerical simulations are finally provided to justify the validity of our channel equalization and estimation algorithms.**

***Index Terms*—OSDM, BEM, doubly-selective channels, channel equalization, channel estimation, underwater acoustic communications.**

I. Introduction

CURRENTLY, multicarrier modulation with orthogonal frequency-division multiplexing (OFDM) and single-carrier modulation with frequency-domain equalization (SC-FDE) are two popular techniques widely used for high-rate wireless communications. OFDM is attractive because it can convert a frequency-selective channel into a set of parallel frequency-flat channels [1], and thus allowing for eliminating inter-symbol interference (ISI) efficiently by simple one-tap equalization on each subcarrier. However, it is well known that OFDM suffers from a large peak-to-average power ratio (PAPR) [2]. In comparison, by performing both the discrete Fourier transform (DFT) and inverse DFT (IDFT) operations at the receiver, SC-FDE has the capability to achieve a lower PAPR [3]. However, its bandwidth and energy management is much more cumbersome than OFDM [4].

As another alternative, orthogonal signal-division multiplexing (OSDM), which was originally proposed in [5], [6], is promising to offer a tradeoff to this dilemma. It is a generalized modulation scheme which connects OFDM and SC-FDE in a unified framework. More specifically, given a transmitted data block of $K = MN$ symbols, OSDM splits the data block into N segments (termed as *vectors* herein) of length M, and its modulation is implemented by M component-wise N-point IDFTs. In this sense, conventional OFDM and SC-FDE can be considered as two extreme cases of OSDM with $M = 1$ and $M = K$, respectively. Moreover, since M and N can be configured otherwise, OSDM has more degrees of freedom in balancing the conflicting system design requirements. It is worth noting that OSDM shares a similar signal structure as vector OFDM, which was independently developed in [7]. They differ only in the cyclic prefix (CP) section [8]. While vector OFDM configures its CP size to be a multiple of the vector length M, OSDM does not have this restriction.[1]

Since the emergence of these modulation schemes is relatively new, so far most existing research has focused on their performance over frequency-selective channels [8]–[14]. Under this scenario, orthogonality can be perfectly maintained among symbol vectors, thus allowing for independent vector-by-vector detection at the receiver. By recognizing this fact, maximum likelihood (ML) vector estimation was applied in [9], [10] and its performance gain was analytically derived in [8], [12]. Although robust to channel fading, the ML receiver incurs a complexity growing exponentially with the vector length M. To ease

Manuscript received April 27, 2018; revised September 25, 2018 and November 23, 2018; accepted December 5, 2018. Date of publication December 17, 2018; date of current version January 4, 2019. The associate editor coordinating the review of this manuscript and approving it for publication was Dr. Xavier Mestre. This work was supported in part by the National Natural Science Foundation of China under Grants 61771394, 61531015, and 61801394, in part by the Natural Science Basic Research Plan in Shaanxi Province of China under Grant 2018JM6042, in part by the Fundamental Research Funds for the Central Universities under Grant 3102017JG05007, and in part by the 111 Project under Grant B18041. *(Corresponding author: Jing Han.)*

J. Han, L. Zhang, and Q. Zhang are with the School of Marine Science and Technology, Northwestern Polytechnical University, Xi'an 710072, China (e-mail: hanj@nwpu.edu.cn; llzhang@nwpu.edu.cn; zhangqf@nwpu.edu.cn).

G. Leus is with the Faculty of Electrical Engineering, Mathematics and Computer Science, Delft University of Technology, Delft 2826 CD, The Netherlands (e-mail: g.j.t.leus@tudelft.nl).

Digital Object Identifier 10.1109/TSP.2018.2887191

[1]That is why we choose the term OSDM in this paper, since here the CP can be of any size longer than the channel delay spread. Another reason for this is that the term OSDM has been adopted in the context of underwater acoustic communications, such as [20], which directly motivates our work.

the computation, linear cancellation and equalization methods were then investigated in [11], [13], respectively, to recover data symbols from ISI. Furthermore, two multiple-antenna extensions with linear equalization were proposed in [14] to collect diversity in the spatial domain.

On the other hand, when the channel is doubly-selective (i.e., both frequency- and time-selective), the Doppler spread destroys the orthogonality of the vectors and thus leads to inter-vector interference (IVI) [15], [16]. It is analogous to inter-carrier interference (ICI) in OFDM, and degrades the system performance significantly. To counteract this effect, an effort was devoted to compensating for carrier phase noise caused by imperfect oscillators [16], [17]. In addition, OSDM has recently also been considered for underwater acoustic (UWA) communications [15], [18]–[20], where due to the severe Doppler effects of UWA channels [21], [22], more emphasis has been placed on IVI mitigation in the receiver design. Meanwhile, several doubly-selective channel models have been adopted to trade off the system performance with the computational complexity.

Specifically, it was assumed in [19] that the time variation over all channel paths can be modeled by a common Doppler scaling factor, under which the Doppler distortion after receiver front-end resampling reduces approximately to a carrier frequency offset (CFO) [23]. As such, null symbols were simply inserted for CFO estimation and compensation. Moreover, to accommodate more general time variation effects in UWA channels, the post-resampling Doppler distortion was modeled as a deterministic time-varying phase in [15] (instead of a single frequency in the CFO case). Accordingly, the OSDM receiver was equipped with iterative per-vector equalization for IVI mitigation. Finally, the complex exponential basis expansion model (CE-BEM) was considered in [20] to take Doppler spreads explicitly into account. It is a more accurate representation of doubly-selective channels, and the proposed OSDM receiver can thus have better Doppler resilience. However, the equalization algorithm in [20] requires direct inversion of channel matrices, which incurs a cubic complexity and may be computationally expensive for practical use.

The aim of this paper is to reduce the computational burden of CE-BEM channel equalization in OSDM systems. Inspired by previous works on OFDM systems [24], [25], we here explore the CE-BEM channel matrix structure and then design low-complexity OSDM equalization algorithms. The main contributions are summarized as follows.

1) *OSDM Signal Model*: With doubly-selective channels approximated by the CE-BEM, it is derived that the composite channel matrix of OSDM systems has a cyclically block-banded structure. Moreover, the blocks in its main band can be further diagonalized by matrix factorization.
2) *OSDM Channel Equalization*: By exploiting the special structure of the composite channel matrix, low-complexity block and serial OSDM equalization algorithms are proposed based on block LDL^H factorization and block iterative matrix inversion, respectively. Both algorithms are implemented in a transformed domain, by which the equalization complexity on each length-M vector can be reduced to the order $\mathcal{O}(M\log_2 M)$.
3) *OSDM Channel Estimation*: A pilot-assisted method is proposed for CE-BEM channel estimation in OSDM systems. It relies on a specifically designed OSDM block structure, where equi-spaced pilot vectors are chosen as frequency-shifted Chu sequences to avoid direct matrix inversion, and surrounded by zeros to eliminate IVI from neighboring data vectors.

The remainder of this paper is organized as follows. Some necessary background of OSDM, as well as its received signal models over frequency- and doubly-selective channels are discussed in Section II. Low-complexity block and serial OSDM equalization algorithms based on the CE-BEM are presented in Section III, and their complexities are provided in Section IV. Doubly-selective channel estimation in OSDM systems is addressed in Section V. The OSDM system performance is then evaluated by numerical simulations in Section VI. Finally, conclusions are drawn in Section VII.

The notation used in this paper is summarized as follows. Bold upper (lower) letters denote matrices (column vectors); $(\cdot)^*$, $(\cdot)^T$, $(\cdot)^H$ and $(\cdot)^\dagger$ stand for conjugate, transpose, Hermitian transpose and Moore-Penrose pseudoinverse, respectively. We define $[\mathbf{x}]_n$ as the nth entry of the vector $\mathbf{x}$, and $[\mathbf{X}]_{m,n}$ as the (m,n)th entry of the matrix $\mathbf{X}$, where all indices are starting from 0. Also, $[\mathbf{x}]_{m:n}$ indicates the subvector of $\mathbf{x}$ from entry m to n, and $[\mathbf{X}]_{m:n,p:q}$ indicates the submatrix of $\mathbf{X}$ from row m to n and from column p to q, where only the colon is kept when all rows or columns are included. We use $\mathrm{diag}\{\mathbf{x}\}$ to represent a diagonal matrix with $\mathbf{x}$ on its diagonal, and $\mathrm{Diag}\{\mathbf{A}_0,\ldots,\mathbf{A}_{N-1}\}$ to represent a block-diagonal matrix created with the submatrices $\{\mathbf{A}_n\}_{n=0}^{N-1}$. Moreover, $\mathbf{0}_{M\times N}$ ($\mathbf{1}_{M\times N}$) denotes the $M\times N$ all-zero (all-one) matrix; $\mathbf{F}_N$ stands for the $N\times N$ unitary DFT matrix, i.e., $[\mathbf{F}_N]_{p,q}=N^{-1/2}e^{-j2\pi pq/N}$; $\mathbf{I}_N$ and $\mathbf{e}_N(n)$ refer to the $N\times N$ identity matrix and its nth column, respectively. Besides, $\mathbf{J}_N$ denotes the $N\times N$ cyclic shift matrix, which is defined as the circulant matrix with its first column $\mathbf{e}_N(1)$. As such, $\mathbf{J}_N^q\mathbf{x}$ is the circularly shifted vector of $\mathbf{x}$ by q entries.

Finally, notice that there are two minor terminological collisions in this paper. First, a block generally indicates a portion of a matrix, while also refering to an OSDM data block. Second, a vector in general stands for a one-dimensional matrix; however, as a specific definition in OSDM, it may also represent a segment in a data block. Which notion is used can always be deduced from the context.

II. Signal Model

Let us consider a transmitted block of K symbols denoted by $\mathbf{d}=[d_0,d_1,\ldots,d_{K-1}]^T$, where the symbols $\{d_k\}$ are drawn from a finite constellation, and are independent and identically distributed (i.i.d.) with unit power, i.e., $\sigma_d^2=1$. To offer a better understanding, we compare the baseband models of OSDM and conventional OFDM in Fig. 1. As a well-known technique, the conventional OFDM system treats the transmitted block $\mathbf{d}$ as a whole, and performs modulation and demodulation at the transceiver by a single K-point IDFT and DFT operation, respectively. On the other hand, by assuming $K=MN$, the

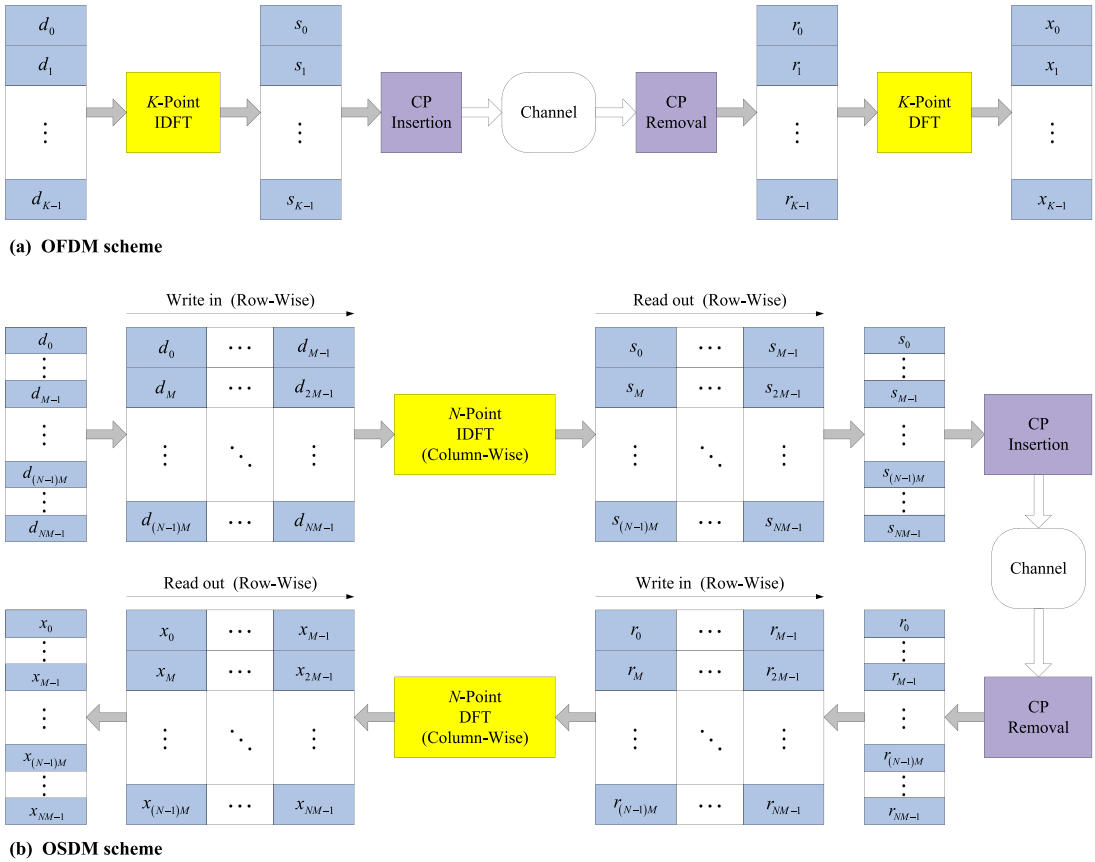

Fig. 1. Comparison between the discrete-time baseband models of OFDM and OSDM.

OSDM system partitions the transmitted block $\mathbf{d}$ into N symbol vectors of length M, i.e.,

$$\mathbf{d}_n = [d_{nM}, d_{nM+1}, \ldots, d_{nM+M-1}]^T \tag{1}$$

for $n = 0, \ldots, N-1$. At the transmitter, the symbols in $\mathbf{d}$ are firstly written row-wise into an $N \times M$ matrix with its nth row filled by the nth symbol vector $\mathbf{d}_n^T$. Then, N-point IDFTs are performed column-wise, and the entries in the resulting matrix are read out row-wise to obtain the length-K transmitted signal $\mathbf{s} = [s_0, s_1, \ldots, s_{K-1}]^T$. As stated in [15], by defining the $K \times K$ permutation matrix

$$\mathbf{P}_{N,M} = \begin{bmatrix} \mathbf{I}_N \otimes \mathbf{e}_M^T(0) \\ \mathbf{I}_N \otimes \mathbf{e}_M^T(1) \\ \vdots \\ \mathbf{I}_N \otimes \mathbf{e}_M^T(M-1) \end{bmatrix} \tag{2}$$

where $\otimes$ stands for the Kronecker product, the OSDM modulation process can be mathematically expressed as

$$\begin{aligned} \mathbf{s} &= \mathbf{P}_{N,M}^H \left(\mathbf{I}_M \otimes \mathbf{F}_N^H\right) \mathbf{P}_{N,M} \mathbf{d} \\ &= \left(\mathbf{F}_N^H \otimes \mathbf{I}_M\right) \mathbf{d}. \end{aligned} \tag{3}$$

In the first line of the above equation, $\mathbf{P}_{N,M}$, $\mathbf{I}_M \otimes \mathbf{F}_N^H$ and $\mathbf{P}_{N,M}^H$ correspond to the row-wise write, N-point IDFT and row-wise read operations, respectively. Subsequently, a CP is inserted at the beginning of each OSDM block to eliminate inter-block interference.

At the receiver, the received signal block after CP removal is denoted by the $K \times 1$ vector $\mathbf{r} = [r_0, r_1, \ldots, r_{K-1}]^T$. OSDM demodulation uses a similar $N \times M$ matrix interleaving operation, and performs N-point DFTs column-wise. Analogous to (3), the OSDM demodulated block can be formulated as

$$\begin{aligned} \mathbf{x} &= \mathbf{P}_{N,M}^H \left(\mathbf{I}_M \otimes \mathbf{F}_N\right) \mathbf{P}_{N,M} \mathbf{r} \\ &= \left(\mathbf{F}_N \otimes \mathbf{I}_M\right) \mathbf{r}. \end{aligned} \tag{4}$$

Before we proceed, two remarks on the OSDM signal structure are now in order.

1) The modulated block in (3) is the same as that of vector OFDM. However, OSDM allows for a more flexible setting of the CP length. Unlike the vector OFDM case, the CP length in OSDM is not restricted to be a multiple of M. It can be any value no less than the maximum discrete delay of the channel [8].
2) As a generalized modulation scheme, OSDM contains conventional OFDM and SC-FDE as its extreme cases. It can be seen from (3) that the OSDM signal structure reduces to that of conventional OFDM and SC-FDE when $M = 1$ and $M = K$, respectively.

A. Precoded-OFDM Interpretation

It is interesting to mention that the OSDM signal in (3) also has a precoded-OFDM interpretation. To see this, we first present a proposition on DFT matrix factorization.

Proposition 1: If $K = MN$, then the $K \times K$ DFT matrix $\mathbf{F}_K$ can be factorized as

$$\mathbf{F}_K = \mathbf{P}_{N,M} \left(\mathbf{I}_N \otimes \mathbf{F}_M \right) \mathbf{\Lambda} \left(\mathbf{F}_N \otimes \mathbf{I}_M \right) \tag{5}$$

where

$$\mathbf{\Lambda} = \mathrm{Diag} \left\{ \mathbf{\Lambda}_M^0, \mathbf{\Lambda}_M^1, \ldots, \mathbf{\Lambda}_M^{N-1} \right\} \tag{6}$$

$$\mathbf{\Lambda}_M^n = \mathrm{diag}\{[1, e^{-j\frac{2\pi n}{K}}, \ldots, e^{-j\frac{2\pi n}{K}(M-1)}]^T\}. \tag{7}$$

Now, by converting the OSDM signal $\mathbf{s}$ into the frequency domain, it can be derived that

$$\mathbf{F}_K \mathbf{s} = \mathbf{P}_{N,M} \begin{bmatrix} \mathbf{F}_M \mathbf{\Lambda}_M^0 \mathbf{d}_0 \\ \mathbf{F}_M \mathbf{\Lambda}_M^1 \mathbf{d}_1 \\ \vdots \\ \mathbf{F}_M \mathbf{\Lambda}_M^{N-1} \mathbf{d}_{N-1} \end{bmatrix}. \tag{8}$$

Recall that, in the case of conventional OFDM, it simply yields $\mathbf{F}_K \mathbf{s} = \mathbf{d}$, which means each symbol is modulated directly on a single subcarrier. In comparison, for OSDM, the symbol vectors $\{\mathbf{d}_n\}$ are precoded by $\{\mathbf{F}_M \mathbf{\Lambda}_M^n\}$, interleaved by $\mathbf{P}_{N,M}$, and then modulated on subcarriers. We can thus consider OSDM as a version of precoded OFDM. The proof of Proposition 1 and (8) can be found in Appendix A.

B. Received Signal Over Frequency-Selective Channels

We proceed to establish the received OSDM signal models. For simplicity, let us first assume the channel to be time-invariant, and denote the equivalent discrete-time channel impulse response (CIR) by the $(L+1) \times 1$ vector $\mathbf{c} = [c_0, c_1, \ldots, c_L]^T$, where L is the channel memory length. In this case, the input-output relationship of the channel is modeled in matrix-vector form as

$$\mathbf{r} = \widetilde{\mathbf{C}} \mathbf{s} + \mathbf{w} \tag{9}$$

where $\widetilde{\mathbf{C}}$ is the $K \times K$ circulant channel matrix with its first column equal to the CIR vector $\mathbf{c}$ appended by $K - L - 1$ zeros; $\mathbf{w}$ is the additive white Gaussian noise term with K entries of zero mean and variance σ^2.

Therefore, based on (3), (4) and (9), the OSDM demodulated block can be written as

$$\mathbf{x} = \mathbf{C} \mathbf{d} + \mathbf{z} \tag{10}$$

where

$$\mathbf{C} = \left(\mathbf{F}_N \otimes \mathbf{I}_M \right) \widetilde{\mathbf{C}} \left(\mathbf{F}_N^H \otimes \mathbf{I}_M \right) \tag{11}$$

is referred to as the composite channel matrix in this paper; $\mathbf{z} = \left(\mathbf{F}_N \otimes \mathbf{I}_M \right) \mathbf{w}$ is the noise term after demodulation. To establish OSDM transmissions over frequency-selective channels, so far there have been a few studies, such as [13], [18], on this issue. The results are summarized here as a proposition to provide a basis for our further derivations.

Proposition 2: Consider an OSDM block with N vectors of length $M = K/N$ transmitted over the time-invariant channel modeled in (9). Define the frequency-domain channel coefficients as

$$H_k = \sum_{l=0}^{L} c_l e^{-j\frac{2\pi}{K} lk}, k = 0, 1, \ldots, K-1. \tag{12}$$

Then, the composite channel matrix has the form

$$\mathbf{C} = \mathrm{Diag} \left\{ \mathbf{H}_0, \mathbf{H}_1, \ldots, \mathbf{H}_{N-1} \right\} \tag{13}$$

where

$$\mathbf{H}_n = \mathbf{\Lambda}_M^{nH} \mathbf{F}_M^H \overline{\mathbf{H}}_n \mathbf{F}_M \mathbf{\Lambda}_M^n \tag{14}$$

$$\overline{\mathbf{H}}_n = \mathrm{diag} \left\{ [H_n, H_{N+n}, \ldots, H_{(M-1)N+n}]^T \right\} \tag{15}$$

for $n = 0, 1, \ldots, N-1$. Furthermore, by dividing $\mathbf{x}$ and $\mathbf{z}$ into N vectors, and defining $\mathbf{x}_n = [\mathbf{x}]_{nM:nM+M-1}$ and $\mathbf{z}_n = [\mathbf{z}]_{nM:nM+M-1}$, it can be obtained that

$$\mathbf{x}_n = \mathbf{H}_n \mathbf{d}_n + \mathbf{z}_n, n = 0, 1, \ldots, N-1. \tag{16}$$

Proof: This proposition can be easily derived from Proposition 1. See our previous work [15, (7), (8), (11) and Appendix A] for a detailed proof. ■

It is well known that conventional OFDM over frequency-selective channels preserves orthogonality of subcarriers and thus channel equalization can be performed independently on each subcarrier. In comparison, as shown in (16), detection of the symbol vectors $\{\mathbf{d}_n\}$ can be similarly decoupled and thus per-vector equalization can be adopted in OSDM [15]. Specifically, since OSDM demodulation in (4) yields a unitary transformation, the demodulated noise $\mathbf{z}$ has the same distribution as $\mathbf{w}$ and it remains white. Therefore, the minimum mean-square error (MMSE) estimate of the nth symbol vector can be expressed as

$$\widehat{\mathbf{d}}_n = \left[\mathbf{H}_n^H \left(\mathbf{H}_n \mathbf{H}_n^H + \sigma^2 \mathbf{I}_M \right)^{-1} \right] \mathbf{x}_n \tag{17}$$

$$= \mathbf{\Lambda}_M^{nH} \mathbf{F}_M^H \left[\overline{\mathbf{H}}_n^H \left(\overline{\mathbf{H}}_n \overline{\mathbf{H}}_n^H + \sigma^2 \mathbf{I}_M \right)^{-1} \right] \mathbf{F}_M \mathbf{\Lambda}_M^n \mathbf{x}_n. \tag{18}$$

Here, note that (18) offers a low-complexity implementation of equalization. This is because, for the direct implementation in (17), the total computational complexity is on the order of $\mathcal{O}(M^3)$. In contrast, the low-complexity equalization in (18) exploits the special structure of $\mathbf{H}_n$ in (14). As a result, only diagonal matrix computations are needed within the brackets in (18). Together with the two frequency shifts and two DFT operations corresponding to $\mathbf{\Lambda}_M^n (\mathbf{\Lambda}_M^{nH})$ and $\mathbf{F}_M (\mathbf{F}_M^H)$, respectively, the total complexity of equalization per vector is only about $\mathcal{O}(M \log_2 M)$.

C. Received Signal Over Doubly-Selective Channels

We now extend our discussion to OSDM transmissions over doubly-selective channels. As a general channel description, let $c_{k,l}$ denote the time-varying CIR at the kth time instant and the lth delay tap. It can be seen that, over an OSDM block of

K symbols, there are as many as $K(L+1)$ CIR coefficients involved, which disables the development of low-complexity equalization. This observation motivates the use of alternative channel models, and in this paper we adopt the CE-BEM to approximate the channel [26], [27].

To be specific, the CE-BEM assumes that the channel time variation at each delay tap is approximately bandlimited and it can be represented as a superposition of $2Q+1$ complex exponential basis functions during each block, i.e., for $k=0,1,\ldots,K-1$ and $l=0,1,\ldots,L$,

$$c_{k,l}=\sum_{q=-Q}^{Q} h_{q,l}e^{j\frac{2\pi}{K}qk} \tag{19}$$

where Q indicates the discrete Doppler spread. The rationale behind (19) is that, at the lth delay tap, instead of representing the channel time variation directly by the K CIR coefficients $\{c_{k,l}\}_{k=0}^{K-1}$ in the time domain, we use the $2Q+1$ BEM coefficients $\{h_{q,l}\}_{q=-Q}^{Q}$ in the Doppler frequency domain. It can be seen that, compared to the CFO and the time-varying phase models in [15], [23], where a common time variation is assumed for all channel paths, the CE-BEM models the time variation on each delay tap independently. Therefore, the CE-BEM can normally achieve a more accurate channel approximation, although bandlimiting the Doppler frequency may also cause a channel modeling error, especially at the edges of each block. Moreover, since $Q \ll K$ in general, the number of channel parameters can be greatly reduced by using the CE-BEM.

The input-output relationship of the doubly-selective channel can be similarly modeled as (9). Based on the CE-BEM in (19), the channel matrix $\widetilde{\mathbf{C}}$ in this case can be rewritten as

$$\widetilde{\mathbf{C}}=\sum_{q=-Q}^{Q}\widetilde{\mathbf{\Gamma}}_K^q\widetilde{\mathbf{G}}_q \tag{20}$$

where $\widetilde{\mathbf{\Gamma}}_K^q=\mathrm{diag}\{[1,e^{j\frac{2\pi}{K}q},\ldots,e^{j\frac{2\pi}{K}q(K-1)}]^T\}$ is the exponential basis matrix; the $K\times K$ coefficient matrix $\widetilde{\mathbf{G}}_q$ is circulant with its first column equal to $\mathbf{h}_q=[h_{q,0},h_{q,1},\ldots,h_{q,L}]^T$ appended by $K-L-1$ zeros. As for the structure of the composite channel matrix $\mathbf{C}$ and the form of the demodulated vector $\mathbf{x}_n$ over the doubly-selective channel, we present our findings in the next proposition.

Proposition 3: Consider an OSDM block with N vectors of length $M=K/N$ transmitted over the time-varying channel modeled by (20). The composite channel matrix in this case has the form

$$\mathbf{C}=\sum_{q=-Q}^{Q}\left(\mathbf{J}_N^q\otimes\mathbf{\Lambda}_M^{-q}\right)\mathbf{G}_q \tag{21}$$

where

$$\mathbf{G}_q=\mathrm{Diag}\left\{\mathbf{H}_{q,0},\mathbf{H}_{q,1},\ldots,\mathbf{H}_{q,N-1}\right\} \tag{22}$$

$$\mathbf{H}_{q,n}=\mathbf{\Lambda}_M^{nH}\mathbf{F}_M^H\overline{\mathbf{H}}_{q,n}\mathbf{F}_M\mathbf{\Lambda}_M^n \tag{23}$$

for $q=-Q,-Q+1,\ldots,Q$ and $n=0,1,\ldots,N-1$, with

$$\overline{\mathbf{H}}_{q,n}=\mathrm{diag}\left\{[H_{q,n},H_{q,N+n},\ldots,H_{q,(M-1)N+n}]^T\right\} \tag{24}$$

and $H_{q,k}=\sum_{l=0}^{L}h_{q,l}e^{-j\frac{2\pi}{K}lk}$ for $k=0,1,\ldots K-1$. Correspondingly, the nth OSDM demodulated vector at the receiver can be written as

$$\mathbf{x}_n=\mathbf{H}_{0,n}\mathbf{d}_n+\sum_{0<|q|\le Q}\mathbf{\Lambda}_M^{-q}\mathbf{H}_{q,(n-q)_N}\mathbf{d}_{(n-q)_N}+\mathbf{z}_n \tag{25}$$

where $(\cdot)_N$ denotes the modulo-N operation.

Proof: See Appendix B. ■

To offer a better understanding, we partition the composite channel matrix $\mathbf{C}$ in (21) into $M\times M$ blocks

$$\mathbf{C}_{n,n'}=[\mathbf{C}]_{nM:nM+M-1,n'M:n'M+M-1} \tag{26}$$

where $n,n'=0,1,\ldots,N-1$, and demonstrate its structure in Fig. 2(a). It can be observed that $\mathbf{C}_{n,n}=\mathbf{H}_{0,n}$, i.e., the blocks on the main block diagonal correspond to Doppler index $q=0$, and $\mathbf{C}_{n,(n-q)_N}=\mathbf{\Lambda}_M^{-q}\mathbf{H}_{q,(n-q)_N}$, i.e., the blocks on the qth lower (upper) block diagonal correspond to Doppler index $q>0$ ($q<0$). We can thus recognize that, if $Q<N/2$, the composite channel matrix $\mathbf{C}$ has a cyclically *block-banded* structure. Furthermore, from Fig. 2(a), we can intuitively understand the OSDM demodulated vector in (25), where the first term models the ISI within one vector and the second term represents the IVI. It is also easy to verify that, for conventional OFDM (i.e., $M=1$), the matrix $\mathbf{C}$ is reduced to a cyclically *scalar-banded* matrix and IVI becomes ICI accordingly.

As for channel equalization, since the symbol vectors in (25) are coupled, the per-vector equalization in (17) cannot be applied over doubly-selective channels. We need to resort back to (10), based on which a straightforward method of MMSE equalization can be written as

$$\widehat{\mathbf{d}}=\mathbf{C}^H\left(\mathbf{C}\mathbf{C}^H+\sigma^2\mathbf{I}_K\right)^{-1}\mathbf{x}. \tag{27}$$

The complexity of this method is dominated by the matrix inversion, which is of order $\mathcal{O}(K^3)$ and can be prohibitive for large K. To alleviate this problem, the D-OSDM method in [20] further organizes the symbol vectors into groups and places Q zero vectors on both sides of each group to decouple them artificially. Although direct matrix inversion is still used, its benefit is to reduce the matrix dimension from K to the group length. Therefore, at the cost of lowering the transmission rate considerably (due to the zero insertion), the D-OSDM method can ease the computational load. However, without exploiting the structure of $\mathbf{C}$, its complexity is still cubic in the group length. To this end, inspired by the low-complexity equalizer design in (18) for frequency-selective channels, a natural question is whether we can take a similar strategy here based on the structure of $\mathbf{C}$ in (21). In fact, Fig. 2(a) sheds some light on solving the problem, and we will focus on the design of low-complexity OSDM equalizers over doubly-selective channels in the following section.

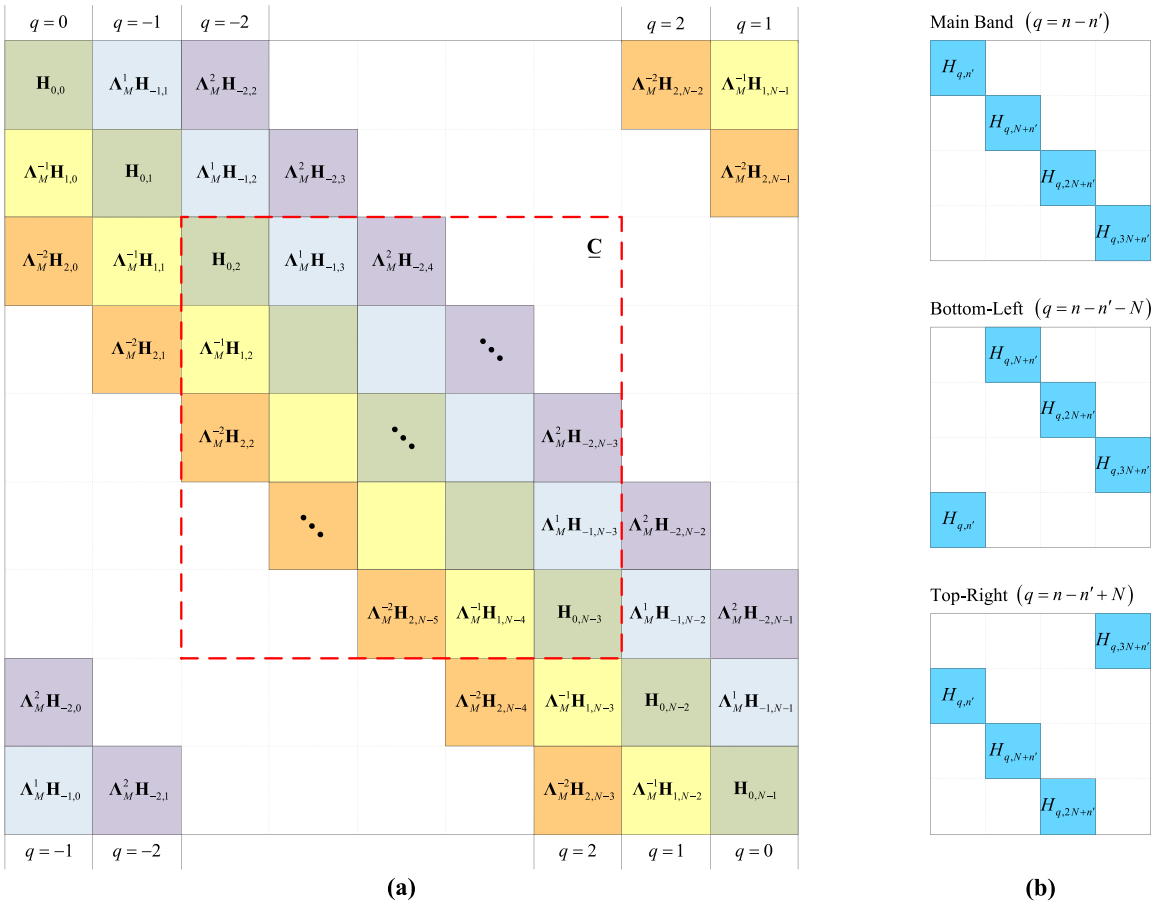

Fig. 2. Structure of $\mathbf{C}$, $\underline{\mathbf{C}}$ and $\overline{\mathbf{C}}_{n,n'}$ with $Q = 2$ and $M = 4$ in (21), (29) and (34), respectively. (a) Structure of $\mathbf{C}$ and $\underline{\mathbf{C}}$. (b) Structures of $\overline{\mathbf{C}}_{n,n'}$.

III. Low-Complexity Equalization

Two low-complexity equalization algorithms are proposed in this section for OSDM transmissions over doubly-selective channels. The first one is similar to (27), which estimates all the symbol vectors (i.e., the whole block) jointly, and thus is referred to as block equalization. In contrast, the second one estimates each symbol vector separately, and thus is termed as serial equalization. Both of them exploit the structure of the composite channel matrix $\mathbf{C}$ to achieve a significant reduction in computational complexity.

To develop the algorithms, throughout this section we make the assumption that $Q < N/2$, which, based on the discussion of Proposition 3, is to guarantee the banded structure of $\mathbf{C}$. In addition, we set the leading and trailing Q vectors of the transmitted block $\mathbf{d}$ to zero vectors, i.e.,

$$\mathbf{d} = \left[\mathbf{0}_{1\times MQ}, \underline{\mathbf{d}}^T, \mathbf{0}_{1\times MQ}\right]^T \tag{28}$$

where $\underline{\mathbf{d}}$ stacks the middle $\underline{N} = N - 2Q$ symbol vectors and denotes the payload part of the transmitted block. By defining the matrix $\mathbf{T} = [\mathbf{I}_K]_{QM:(N-Q)M-1,:}$, it can be expressed as $\underline{\mathbf{d}} = \mathbf{T}\mathbf{d}$. Meanwhile, note that instead of placing zero vectors around each vector group as in [20], here they are inserted only at the edges of the entire block. In other words, all symbol vectors in the block are organized as one group. As a result, the overhead thus incurred is reduced to the minimum.

A. Block Equalization

For block equalization, the OSDM demodulated block in (10) is similarly truncated by $\mathbf{T}$, and has the form

$$\underline{\mathbf{x}} = \underline{\mathbf{C}}\,\underline{\mathbf{d}} + \underline{\mathbf{z}} \tag{29}$$

where $\underline{\mathbf{x}} = \mathbf{T}\mathbf{x}$, $\underline{\mathbf{z}} = \mathbf{T}\mathbf{z}$, and $\underline{\mathbf{C}} = \mathbf{T}\mathbf{C}\mathbf{T}^H$ is the $M\underline{N} \times M\underline{N}$ submatrix at the center of $\mathbf{C}$ [see Fig. 2(a)]. By eliminating the top-right and bottom-left corners of $\mathbf{C}$, the cyclic coupling effect is removed from $\underline{\mathbf{x}}$, and the remaining matrix $\underline{\mathbf{C}}$ typically has a standard (not cyclically) block-banded structure. Note though that we should also pay attention to the special case when $Q \geq \underline{N} - 1$, in which $\underline{\mathbf{C}}$ is actually a full matrix. For convenience and with a slight abuse of terminology, we consider $\underline{\mathbf{C}}$ as a block-banded matrix with block semi-bandwidth (BSB)

$$\beta_C = \min\{Q, \underline{N} - 1\}. \tag{30}$$

Then, based on (29), block MMSE equalization for OSDM takes the form

$$\widehat{\underline{\mathbf{d}}} = \underline{\mathbf{C}}^H \left(\underline{\mathbf{C}}\,\underline{\mathbf{C}}^H + \sigma^2 \mathbf{I}_{M\underline{N}}\right)^{-1} \underline{\mathbf{x}}. \tag{31}$$

This equation can be considered as a truncated version of (27). Moreover, from (30), it is easy to verify that here the matrix $\underline{\mathbf{R}} = \underline{\mathbf{C}}\,\underline{\mathbf{C}}^H + \sigma^2 \mathbf{I}_{M\underline{N}}$ is also block-banded with BSB

$$\beta_R = \min\{2Q, \underline{N} - 1\}. \tag{32}$$

Given the fact that any block-banded matrix is also scalar-banded, a straightforward approach to efficiently compute $\underline{\mathbf{R}}^{-1}$ in this case is to treat $\underline{\mathbf{R}}$ as a scalar-banded matrix with semi-bandwidth $M\beta_R + M - 1$. Then, the band LDL^H factorization algorithm in [25] can be adopted to implement the block equalizer in (31). Unfortunately, the complexity of this algorithm, being of order $\mathcal{O}(\beta_R^2 M^3 \underline{N})$, is still cubic in M and thus may be impractical to use in OSDM systems with large vector sizes.

In order to reduce the equalization complexity, we further investigate the structure of the blocks in $\mathbf{C}$. To this end, we establish the following proposition.

Proposition 4: Within the composite channel matrix $\mathbf{C}$ in (21), every nonzero block $\mathbf{C}_{n,n'}$ defined in (26) can be factorized as

$$\mathbf{C}_{n,n'} = \mathbf{\Lambda}_M^{nH} \mathbf{F}_M^H \overline{\mathbf{C}}_{n,n'} \mathbf{F}_M \mathbf{\Lambda}_M^{n'}, \tag{33}$$

where

$$\overline{\mathbf{C}}_{n,n'} = \begin{cases} \overline{\mathbf{H}}_{n-n',n'}, & \text{if } |n-n'| \le Q \\ \mathbf{J}_M^{-1} \overline{\mathbf{H}}_{n-n'-N,n'}, & \text{if } N-Q \le n-n' \le N-1 \\ \mathbf{J}_M^{1} \overline{\mathbf{H}}_{n-n'+N,n'}, & \text{if } 1-N \le n-n' \le Q-N. \end{cases} \tag{34}$$

Proof: See Appendix C. ■

Note that the three forms of $\mathbf{C}_{n,n'}$ in (33) and (34) are located in the main block band, bottom-left and top-right corners of $\mathbf{C}$, respectively. For clarity, we also illustrate the structure of $\overline{\mathbf{C}}_{n,n'}$ in Fig. 2(b). It can be seen that only $\mathbf{C}_{n,n'}$ in the main block band can be diagonalized. Moreover, by selecting the central part of $\mathbf{C}$, the matrix $\underline{\mathbf{C}}$ contains only such kind of blocks. Inspired by the above observations, we propose the following block equalization algorithm for OSDM.

Theorem 1: The truncated composite channel matrix $\underline{\mathbf{C}}$ in (29) can be factorized as

$$\underline{\mathbf{C}} = \underline{\mathbf{\Lambda}}^H \left(\mathbf{I}_{\underline{N}} \otimes \mathbf{F}_M^H\right) \underline{\overline{\mathbf{C}}} \left(\mathbf{I}_{\underline{N}} \otimes \mathbf{F}_M\right) \underline{\mathbf{\Lambda}} \tag{35}$$

where $\underline{\mathbf{\Lambda}} = \mathbf{T}\mathbf{\Lambda}\mathbf{T}^H = \mathrm{Diag}\{\mathbf{\Lambda}_M^Q, \ldots, \mathbf{\Lambda}_M^{N-Q-1}\}$, and $\underline{\overline{\mathbf{C}}} = \mathbf{T}\overline{\mathbf{C}}\mathbf{T}^H$ with $\overline{\mathbf{C}}$ being the $K \times K$ matrix composed of the blocks in (34). Accordingly, the block MMSE equalization of OSDM in (31) can be reformulated as

$$\widehat{\underline{\mathbf{d}}} = \underline{\mathbf{\Lambda}}^H \left(\mathbf{I}_{\underline{N}} \otimes \mathbf{F}_M^H\right) \left[\underline{\overline{\mathbf{C}}}^H \left(\underline{\overline{\mathbf{C}}}\,\underline{\overline{\mathbf{C}}}^H + \sigma^2 \mathbf{I}_{M\underline{N}}\right)^{-1}\right] \times \left(\mathbf{I}_{\underline{N}} \otimes \mathbf{F}_M\right) \underline{\mathbf{\Lambda}}\underline{\mathbf{x}}. \tag{36}$$

Moreover, $\underline{\overline{\mathbf{C}}}$ and $\underline{\overline{\mathbf{R}}} = \underline{\overline{\mathbf{C}}}\,\underline{\overline{\mathbf{C}}}^H + \sigma^2 \mathbf{I}_{M\underline{N}}$ are diagonal-block-banded (DBB) matrices with the same block size and bandwidth as $\underline{\mathbf{C}}$ and $\underline{\mathbf{R}}$, i.e., β_C and β_R, respectively.

Proof: Based on Proposition 4, we can readily verify (35). Then, substituting (35) into (31), and given the fact that $\left(\mathbf{I}_{\underline{N}} \otimes \mathbf{F}_M\right) \underline{\mathbf{\Lambda}}$ is a unitary matrix, we can obtain (36). Also, the DBB structure of $\underline{\overline{\mathbf{C}}}$ and $\underline{\overline{\mathbf{R}}}$ can be easily identified, since

$$\underline{\overline{\mathbf{C}}}_{n,n'} = \overline{\mathbf{C}}_{n+Q,n'+Q} = \begin{cases} \overline{\mathbf{H}}_{n-n',n'+Q}, & \text{if } |n-n'| \le \beta_C \\ \mathbf{0}_{M\times M}, & \text{otherwise} \end{cases} \tag{37}$$

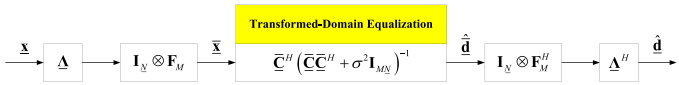

Fig. 3. Proposed block equalization scheme for OSDM.

for $0 \le n, n' \le \underline{N}$, where $\underline{\overline{\mathbf{C}}}_{n,n'}$ is the (n,n')th block in $\underline{\overline{\mathbf{C}}}$ defined similarly to (26). ■

According to (36), the structure of the block equalization algorithm is shown in Fig. 3, which consists of three steps:

1) Generate a transformed version of the demodulated block, i.e., $\underline{\overline{\mathbf{x}}} = \left(\mathbf{I}_{\underline{N}} \otimes \mathbf{F}_M\right) \underline{\mathbf{\Lambda}}\,\underline{\mathbf{x}}$, by performing the frequency shift $\mathbf{\Lambda}_n$ and then the DFT $\mathbf{F}_M$ on each vector $\underline{\mathbf{x}}_n$;
2) Equalize the demodulated block in the transformed domain, i.e., $\widehat{\underline{\overline{\mathbf{d}}}} = [\underline{\overline{\mathbf{C}}}^H (\underline{\overline{\mathbf{C}}}\,\underline{\overline{\mathbf{C}}}^H + \sigma^2 \mathbf{I}_{M\underline{N}})^{-1}]\underline{\overline{\mathbf{x}}}$;
3) Transform it back and obtain the final estimate of the symbol block $\widehat{\underline{\mathbf{d}}} = \underline{\mathbf{\Lambda}}^H \left(\mathbf{I}_{\underline{N}} \otimes \mathbf{F}_M^H\right) \widehat{\underline{\overline{\mathbf{d}}}}$.

Moreover, from Theorem 1, we know that $\underline{\overline{\mathbf{R}}}$ is block-banded and all its nonzero blocks are diagonal. Therefore, instead of inverting $\underline{\mathbf{R}}$ as a general scalar-banded matrix in the block equalizer in (31), here the DBB structure of $\underline{\overline{\mathbf{R}}}$ can be further exploited to lower the complexity of the block equalizer in (36). To make this clear, we first extend the scalar LDL^H factorization algorithm in [25] to a block version, and present the following theorem.

Theorem 2: Let $\mathbf{R}$ be an $MN \times MN$ positive-definite matrix that is partitioned into blocks of size $M \times M$. Its block LDL^H factorization can be written as

$$\mathbf{R} = \mathbf{L}\mathbf{D}\mathbf{L}^H \tag{38}$$

where $\mathbf{L}$ and $\mathbf{D}$ are block-lower-triangular and block-diagonal matrices, respectively, with blocks of the same size as those in $\mathbf{R}$. Moreover, it can be shown that

1) Such factorization always exists; in addition, by restricting the blocks on the main block diagonal of $\mathbf{L}$ to the identity matrix $\mathbf{I}_M$, the factorization is also unique.
2) If $\mathbf{R}$ is block-banded, then $\mathbf{L}$ and $\mathbf{R}$ have the same BSB.
3) If all nonzero blocks in $\mathbf{R}$ are diagonal, so are the nonzero blocks in $\mathbf{L}$ and $\mathbf{D}$.

Proof: These statements can be proved similarly as their corresponding conclusions for scalar LDL^H factorization in [32]. We thus omit the details here for briefness. ■

We now focus on the special case where $\mathbf{R} = \underline{\overline{\mathbf{R}}}$, which is a positive-definite and DBB matrix. For this case, an iterative algorithm is developed for the block LDL^H factorization $\underline{\overline{\mathbf{R}}} = \underline{\overline{\mathbf{L}}}\,\underline{\overline{\mathbf{D}}}\,\underline{\overline{\mathbf{L}}}^H$ as shown in Algorithm 1. Here, based on Theorem 2, we can easily make two observations. First, $\underline{\overline{\mathbf{L}}}$ is block-banded. As a result, there is no need to compute all the blocks $\underline{\overline{\mathbf{L}}}_{n,n'}, 0 \le n' < n \le \underline{N}$, since, for any given n, only $\min\{\beta_R, n\}$ nonzero blocks exist below the main diagonal of $\underline{\overline{\mathbf{L}}}$. Second, all the blocks in $\underline{\overline{\mathbf{L}}}$ and $\underline{\overline{\mathbf{D}}}$ are diagonal. Therefore, each matrix operation (including the matrix inversion) in lines 6 and 8 of Algorithm 1 requires only M complex operations.

Based on the block LDL^H factorization $\underline{\overline{\mathbf{R}}} = \underline{\overline{\mathbf{L}}}\,\underline{\overline{\mathbf{D}}}\,\underline{\overline{\mathbf{L}}}^H$ described above, the transformed-domain equalization in Fig. 3 has a low-complexity implementation, whose procedure is listed in

Algorithm 1: Block LDL^H Factorization.

Definitions: $\overline{\underline{\mathbf{R}}}_{n,n'}$, $\overline{\underline{\mathbf{L}}}_{n,n'}$ and $\overline{\underline{\mathbf{D}}}_{n,n'}$ are the (n,n')th blocks of $\overline{\underline{\mathbf{R}}}$, $\overline{\underline{\mathbf{L}}}$ and $\overline{\underline{\mathbf{D}}}$, respectively.

1: Initialize the blocks $\overline{\underline{\mathbf{L}}}_{0,0} = \mathbf{I}_M$ and $\overline{\underline{\mathbf{D}}}_{0,0} = \overline{\underline{\mathbf{R}}}_{0,0}$.
2: **for** $n = 1 : \underline{N} - 1$ **do**
3: Enforce the identity-block constraint: $\overline{\underline{\mathbf{L}}}_{n,n} = \mathbf{I}_M$.
4: Determine the number of nonzero blocks:

$$\beta = \min\{\beta_R,\, n\}.$$

5: **for** $n' = n - \beta : n - 1$ **do**
6: Compute the nonzero blocks in $\overline{\underline{\mathbf{L}}}$:

$$\overline{\underline{\mathbf{L}}}_{n,n'} = \left(\overline{\underline{\mathbf{R}}}_{n,n'} - \sum_{i=n-\beta}^{n'-1} \overline{\underline{\mathbf{L}}}_{n,i}\overline{\underline{\mathbf{D}}}_{i,i}\overline{\underline{\mathbf{L}}}_{n',i}^{H}\right)\overline{\underline{\mathbf{D}}}_{n',n'}^{-1}.$$

7: **end for**
8: Compute the block on the main diagonal of $\overline{\underline{\mathbf{D}}}$:

$$\overline{\underline{\mathbf{D}}}_{n,n} = \overline{\underline{\mathbf{R}}}_{n,n} - \sum_{i=n-\beta}^{n-1} \overline{\underline{\mathbf{L}}}_{n,i}\overline{\underline{\mathbf{D}}}_{i,i}\overline{\underline{\mathbf{L}}}_{n,i}^{H}.$$

9: **end for**

Algorithm 2: Transformed-domain Equalization.

1: Construct the DBB matrix $\overline{\underline{\mathbf{R}}}$.
2: Perform the block factorization $\overline{\underline{\mathbf{R}}} = \overline{\underline{\mathbf{L}}}\,\overline{\underline{\mathbf{D}}}\,\overline{\underline{\mathbf{L}}}^{H}$ by running Algorithm 1, and obtain $\overline{\underline{\mathbf{L}}}$ and $\overline{\underline{\mathbf{D}}}$.
3: Solve the linear system $\overline{\underline{\mathbf{x}}} = \overline{\underline{\mathbf{R}}}\mathbf{y}$ in three steps:
4: (1) Solve the block-lower-triangular system $\overline{\underline{\mathbf{x}}} = \overline{\underline{\mathbf{L}}}\mathbf{y}'$.
5: (2) Solve the block-diagonal system $\mathbf{y}' = \overline{\underline{\mathbf{D}}}\mathbf{y}''$.
6: (3) Solve the block-upper-triangular system $\mathbf{y}'' = \overline{\underline{\mathbf{L}}}^{H}\mathbf{y}$.
7: Obtain the estimate of the symbol block $\overline{\underline{\mathbf{d}}}$ in the transformed domain: $\widehat{\overline{\underline{\mathbf{d}}}} = \overline{\underline{\mathbf{C}}}^{H}\mathbf{y}$.

Algorithm 2. Note that, since the two block-triangular systems in lines 4 and 6 are banded, we can easily utilize a block version of the band forward and backward substitution algorithms to solve them. Moreover, thanks to the diagonal structure of the blocks in $\overline{\underline{\mathbf{L}}}$ and $\overline{\underline{\mathbf{D}}}$, the total complexity of the block equalization in Algorithm 2 is only linear in $M\underline{N}$. A more detailed discussion on the computational complexity will be presented in Section IV.

B. Serial Equalization

As mentioned above, serial equalization of OSDM is performed on a vector-by-vector basis. Suppose we want to estimate the nonzero symbol vector $\mathbf{d}_n$ in the transmitted block (28), where $n \in \{Q, Q+1, \ldots, N-Q-1\}$. From the structure of the composite channel matrix $\mathbf{C}$ shown in Fig. 2, it can be seen that the energy of $\mathbf{d}_n$ spreads over its neighboring $2Q+1$ vectors. We can thus obtain

$$\underline{\mathbf{x}}_n = \underline{\mathbf{C}}_n\underline{\mathbf{d}}_n + \underline{\mathbf{z}}_n \tag{39}$$

where $\underline{\mathbf{x}}_n = [\mathbf{x}_{n-Q}^T, \ldots, \mathbf{x}_{n+Q}^T]^T$, $\underline{\mathbf{z}}_n = [\mathbf{z}_{n-Q}^T, \ldots, \mathbf{z}_{n+Q}^T]^T$, $\underline{\mathbf{d}}_n = [\mathbf{d}_{n-2Q}^T, \ldots, \mathbf{d}_{n+2Q}^T]^T$, and

$$\underline{\mathbf{C}}_n = \begin{bmatrix} \mathbb{C}_{n-Q,n-2Q} & \cdots & \mathbb{C}_{n-Q,n} & & \\ & \ddots & \ddots & \ddots & \\ & & \mathbb{C}_{n+Q,n} & \cdots & \mathbb{C}_{n+Q,n+2Q} \end{bmatrix} \tag{40}$$

is a (non-square) block-banded matrix with at most $2Q+1$ nonzero blocks on each block row. It is easy to verify that these nonzero blocks generally have the form $\mathbb{C}_{i,j} = \mathbf{C}_{i,j}$, for $n - Q \le i \le n + Q$ and $n - 2Q \le j \le n + 2Q$, and the index j here should be taken modulo-N. However, thanks to the leading and trailing zero vectors in the transmitted block, the cyclic coupling effect is eliminated among the edge vectors, and thus $\{\mathbb{C}_{i,j} \,|\, j < Q \text{ or } j > N - Q - 1\}$ in (40) can be further set to zero to ease the computation. Therefore, it yields

$$\mathbb{C}_{i,j} = \begin{cases} \mathbf{C}_{i,j}, & \text{if } Q \le j \le N - Q - 1 \\ \mathbf{0}_{M\times M}, & \text{otherwise.} \end{cases} \tag{41}$$

Base on this, serial equalization can be applied to produce the symbol vector estimate

$$\widehat{\mathbf{d}}_n = \underline{\mathcal{C}}_n^H\left(\underline{\mathbf{C}}_n\underline{\mathbf{C}}_n^H + \sigma^2\mathbf{I}_{M(2Q+1)}\right)^{-1}\underline{\mathbf{x}}_n \tag{42}$$

where $\underline{\mathcal{C}}_n = [\underline{\mathbf{C}}_n]_{:,2QM:2QM+M-1}$.

Similar to the block equalization in (31), direct computation of (42) involves inverting $\underline{\mathbf{R}}_n = \underline{\mathbf{C}}_n\underline{\mathbf{C}}_n^H + \sigma^2\mathbf{I}_{M(2Q+1)}$ and requires a cubic complexity. Therefore, as a counterpart of Theorem 1, we establish the following result to achieve low-complexity serial equalization.

Theorem 3: The matrix $\underline{\mathbf{C}}_n$ in (39) can be factorized as

$$\underline{\mathbf{C}}_n = \underline{\mathbf{\Lambda}}_n^H\left(\mathbf{I}_{2Q+1}\otimes\mathbf{F}_M^H\right)\overline{\underline{\mathbf{C}}}_n\left(\mathbf{I}_{4Q+1}\otimes\mathbf{F}_M\right)\underline{\mathbf{\Lambda}}_n^+ \tag{43}$$

where $\underline{\mathbf{\Lambda}}_n = \mathrm{Diag}\{\mathbf{\Lambda}_M^{n-Q}, \ldots, \mathbf{\Lambda}_M^{n+Q}\}$, $\underline{\mathbf{\Lambda}}_n^+ = \mathrm{Diag}\{\mathbf{\Lambda}_M^{n-2Q}, \ldots, \mathbf{\Lambda}_M^{n+2Q}\}$, and $\overline{\underline{\mathbf{C}}}_n$ has the same structure as $\underline{\mathbf{C}}_n$ with blocks $\{\mathbb{C}_{i,j}\}$ replaced by

$$\overline{\mathbb{C}}_{i,j} = \begin{cases} \overline{\mathbf{C}}_{i,j}, & \text{if } Q \le j \le N - Q - 1 \\ \mathbf{0}_{M\times M}, & \text{otherwise.} \end{cases} \tag{44}$$

Accordingly, the serial MMSE equalization of OSDM in (42) can be reformulated as

$$\widehat{\mathbf{d}}_n = \mathbf{\Lambda}_M^{nH}\mathbf{F}_M^H\left[\overline{\underline{\mathcal{C}}}_n^H\left(\overline{\underline{\mathbf{C}}}_n\overline{\underline{\mathbf{C}}}_n^H + \sigma^2\mathbf{I}_{M(2Q+1)}\right)^{-1}\right] \times\left(\mathbf{I}_{2Q+1}\otimes\mathbf{F}_M\right)\underline{\mathbf{\Lambda}}_n\underline{\mathbf{x}}_n \tag{45}$$

where $\overline{\underline{\mathcal{C}}}_n = [\overline{\underline{\mathbf{C}}}_n]_{:,2QM:2QM+M-1}$. Moreover, when $n = Q, Q+1, \ldots, N-Q-1$, $\overline{\underline{\mathbf{R}}}_n = \overline{\underline{\mathbf{C}}}_n\overline{\underline{\mathbf{C}}}_n^H + \sigma^2\mathbf{I}_{M(2Q+1)}$ has a special structure with all its $M\times M$ blocks $[\overline{\underline{\mathbf{R}}}_n]_{qM:qM+M-1,q'M:q'M+M-1}$, for $q, q' = 0, 1, \ldots, 2Q$, being diagonal.

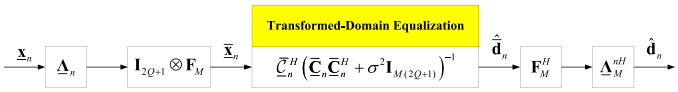

Fig. 4. Proposed serial equalization scheme for OSDM.

Proof: It can be seen that, as $\overline{\mathbf{C}}$ in block equalization, $\underline{\overline{\mathbf{C}}}_n$ here contains only the blocks of the first kind in (34), i.e., all nonzero blocks in $\underline{\overline{\mathbf{C}}}_n$ are diagonal. With this observation, the proof is similar to that of Theorem 1 and thus omitted. ■

Theorem 3 suggests that, instead of a direct implementation as in (42), the serial equalization may be able to achieve a lower complexity by adopting (45). Similar to the block equalization in Fig. 3, it can be implemented as shown in Fig. 4. Here, the vector $\underline{\overline{\mathbf{x}}}_n = (\mathbf{I}_{2Q+1} \otimes \mathbf{F}_M)\underline{\mathbf{\Lambda}}_n \underline{\mathbf{x}}_n$ is first generated, then it is equalized in the transformed domain as $\underline{\widehat{\overline{\mathbf{d}}}}_n = \underline{\overline{\mathcal{C}}}_n^H (\underline{\overline{\mathbf{C}}}_n \underline{\overline{\mathbf{C}}}_n^H + \sigma^2 \mathbf{I}_{M(2Q+1)})^{-1} \underline{\overline{\mathbf{x}}}_n$, and finally the estimate of the nth symbol vector is obtained by an inverse transform, i.e., $\widehat{\mathbf{d}}_n = \mathbf{\Lambda}_M^{nH} \mathbf{F}_M^H \widehat{\overline{\mathbf{d}}}_n$.

To compute $\underline{\overline{\mathbf{R}}}_n^{-1}$ for serial OSDM equalization, we do not employ the block LDL^H factorization algorithm given in Section III-A. Instead, we extend the iterative matrix inversion algorithm in [28]. Specifically, we partition $\underline{\overline{\mathbf{R}}}_{n-1}$ and $\underline{\overline{\mathbf{R}}}_n$ as

$$\underline{\overline{\mathbf{R}}}_{n-1} = \begin{bmatrix} \mathbf{U}_{n-1} & \mathbf{\Theta}_{n-1}^H \\ \mathbf{\Theta}_{n-1} & \mathbf{\Sigma}_n \end{bmatrix}, \quad \underline{\overline{\mathbf{R}}}_n = \begin{bmatrix} \mathbf{\Sigma}_n & \widetilde{\mathbf{\Theta}}_n \\ \widetilde{\mathbf{\Theta}}_n^H & \widetilde{\mathbf{U}}_n \end{bmatrix} \tag{46}$$

where $\mathbf{U}_{n-1}$ and $\widetilde{\mathbf{U}}_n$ are $M \times M$ matrices, $\mathbf{\Theta}_{n-1}$ and $\widetilde{\mathbf{\Theta}}_n$ are $2QM \times M$ matrices, and $\mathbf{\Sigma}_n$ is the common $2QM \times 2QM$ matrix in $\underline{\overline{\mathbf{R}}}_{n-1}$ and $\underline{\overline{\mathbf{R}}}_n$. Similarly, the partitioning scheme (with the same 2×2 block dimensions) is also adopted for their inverses, i.e.,

$$\underline{\overline{\mathbf{R}}}_{n-1}^{-1} = \begin{bmatrix} \mathbf{V}_{n-1} & \mathbf{\Phi}_{n-1}^H \\ \mathbf{\Phi}_{n-1} & \mathbf{\Xi}_{n-1} \end{bmatrix}, \quad \underline{\overline{\mathbf{R}}}_n^{-1} = \begin{bmatrix} \widetilde{\mathbf{\Xi}}_n & \widetilde{\mathbf{\Phi}}_n \\ \widetilde{\mathbf{\Phi}}_n^H & \widetilde{\mathbf{V}}_n \end{bmatrix}. \tag{47}$$

Based on (46) and (47), the block iterative algorithm of computing $\{\underline{\overline{\mathbf{R}}}_n^{-1}\}$ is summarized in Algorithm 3, and the related derivations are presented in Appendix D. The main idea is to exploit the existence of the common block $\mathbf{\Sigma}_n$ to save computations. Similar to the block equalization case, the serial equalization is roughly of linear complexity in $M\underline{N}$. We will provide its complexity analysis in Section IV.

Algorithm 3: Block Iterative Matrix Inversion.

1: Compute $\underline{\overline{\mathbf{R}}}_Q$ and its inverse $\underline{\overline{\mathbf{R}}}_Q^{-1}$.
2: **for** $n = Q+1 : N-Q-1$ **do**
3: (1) Update the matrix $\underline{\overline{\mathbf{R}}}_n$:
4: **for** $q = 0 : 2Q-1$ **do**
5: $\left[\widetilde{\mathbf{\Theta}}_n\right]_{qM:qM+M-1,:} = \sum_{i=0}^{q} \overline{\mathbb{C}}_{n-Q+q,n+i} \overline{\mathbb{C}}_{n+Q,n+i}^H$
6: **end for**
7: $\widetilde{\mathbf{U}}_n = \sigma^2 \mathbf{I}_M + \sum_{i=0}^{2Q} \overline{\mathbb{C}}_{n+Q,n+i} \overline{\mathbb{C}}_{n+Q,n+i}^H$
8: (2) Compute the matrix $\mathbf{\Sigma}_n^{-1}$:
9: $\mathbf{\Sigma}_n^{-1} = \mathbf{\Xi}_{n-1} - \mathbf{\Phi}_{n-1} \mathbf{V}_{n-1}^{-1} \mathbf{\Phi}_{n-1}^H$
10: (3) Update the matrix $\underline{\overline{\mathbf{R}}}_n^{-1}$:
11: $\mathbf{\Omega}_n = -\mathbf{\Sigma}_n^{-1} \widetilde{\mathbf{\Theta}}_n$
12: $\widetilde{\mathbf{V}}_n = \left(\widetilde{\mathbf{U}}_n + \widetilde{\mathbf{\Theta}}_n^H \mathbf{\Omega}_n\right)^{-1}$
13: $\widetilde{\mathbf{\Phi}}_n = \mathbf{\Omega}_n \widetilde{\mathbf{V}}_n$
14: $\widetilde{\mathbf{\Xi}}_n = \mathbf{\Sigma}_n^{-1} + \mathbf{\Omega}_n \widetilde{\mathbf{V}}_n \mathbf{\Omega}_n^H$
15: **end for**

IV. Computational Complexity

Compared to the equalization methods in (31) and (42) using direct matrix inversions, the block and serial OSDM equalization algorithms proposed in this paper are based on the channel matrix factorizations in (35) and (43), respectively, and thus operate in the transformed domain. By this means, the proposed algorithms can achieve a much lower complexity by exploiting the special matrix structures described in Theorems 1 and 3. In this section, we present a detailed complexity analysis to make this clearer.

A. Block Equalization

Let us begin with evaluating the complexity of Algorithm 2. Since all its operations are in block form (with block size $M \times M$), for simplicity the complexity is first measured in terms of block additions (BAs), block multiplications (BMs), and block inversions (BIs). Thanks to the banded structure of $\underline{\overline{\mathbf{C}}}$, constructing $\underline{\overline{\mathbf{R}}}$ in line 1 does not need $\mathcal{O}(\underline{N}^3)$ block operations; instead, it costs only $(2Q^2+Q+1)\underline{N}$ BAs and $(2Q^2+3Q+1)\underline{N}$ BMs. Moreover, since the banded structure is inherited by $\underline{\overline{\mathbf{R}}}$, the block LDL^H factorization $\underline{\overline{\mathbf{R}}} = \underline{\overline{\mathbf{L}}}\underline{\overline{\mathbf{D}}}\underline{\overline{\mathbf{L}}}^H$ in line 2 can thus use a banded algorithm as in Algorithm 1, which requires $(2Q^2+Q)\underline{N}$ BAs, $(2Q^2+3Q)\underline{N}$ BMs and $2Q\underline{N}$ BIs. Similarly, the three-step solution of $\underline{\overline{\mathbf{x}}} = \underline{\overline{\mathbf{R}}}\mathbf{y}$ in lines 3–6 can be implemented by band forward and backward substitution algorithms, which involves $4Q\underline{N}$ BAs, $4Q\underline{N}$ BMs and $\underline{N}$ BIs. In addition, the symbol block estimation in line 7 produces $2Q\underline{N}$ BAs and $(2Q+1)\underline{N}$ BMs.[2]

Then, given the fact that the blocks in $\underline{\overline{\mathbf{C}}}$ and $\underline{\overline{\mathbf{R}}}$ are diagonal, we can readily have that one BA, BM and BI correspond to M complex additions (CAs), complex multiplications (CMs) and complex divisions (CDs), respectively. Therefore, Algorithm 2 actually has a linear complexity in $M\underline{N}$.

B. Serial Equalization

For serial equalization, we focus first on the complexity of Algorithm 3. During the initialization in line 1, constructing $\underline{\overline{\mathbf{R}}}_Q$ requires $\mathcal{O}(Q^3)$ block operations, which corresponds to a complexity on the order of $\mathcal{O}(Q^3 M)$. Meanwhile, since $\underline{\overline{\mathbf{R}}}_Q$ contains only $M \times M$ diagonal blocks, its inversion can be decomposed into M matrix inversions of a small size $(2Q+1) \times (2Q+1)$, incurring also a $\mathcal{O}(Q^3 M)$ complexity. Furthermore, in the main loop of Algorithm 3, updating $\underline{\overline{\mathbf{R}}}_n$ in lines 4–7 requires $2Q^2+Q+1$ BAs and $2Q^2+3Q+1$ BMs; computing $\mathbf{\Sigma}_n^{-1}$ in

[2]Note that the complexity of Algorithm 2 computed here is slightly larger than its exact value, since we ignore the bandwidth truncation at the top-left and bottom-right corners of banded matrices for simplicity.

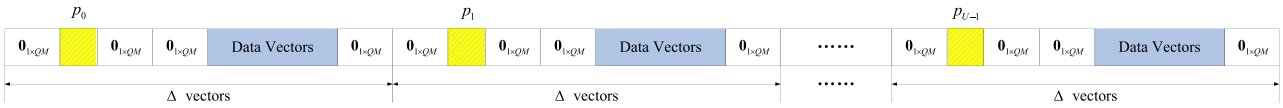

Fig. 5. OSDM block structure for channel estimation.

TABLE I
COMPLEXITY OF THE PROPOSED OSDM EQUALIZATION ALGORITHMS

Type		Complexity
Block Equalization	CA	$\left(2\log_2 M + 4Q^2 + 8Q + 1\right) M\underline{N}$
	CM	$\left(\log_2 M + 4Q^2 + 12Q + 4\right) M\underline{N}$
	CD	$(2Q+1)\, M\underline{N}$
Serial Equalization	CA	$\left(2\log_2 M + 14Q^2 + 7Q + 1\right) M\underline{N}$
	CM	$\left(\log_2 M + 14Q^2 + 15Q + 5\right) M\underline{N}$
	CD	$(2Q+1)\, M\underline{N}$

line 9 requires $2Q^2+Q$ BAs, $2Q^2+Q$ BMs and $2Q$ BIs; updating $\overline{\mathbf{R}}_n^{-1}$ in lines 11–14 requires $6Q^2+Q$ BAs, $6Q^2+5Q$ BMs and one BI. Then, on top of Algorithm 3, another $4Q^2+4Q$ BAs and $4Q^2+6Q+2$ BMs are required to obtain the vector $\widehat{\overline{\mathbf{d}}}_n$. It can be seen that, similar to the block equalization case, in the transformed domain the complexity of the serial equalization (for all $\underline{N}$ data symbol vectors) is roughly[3] linear in $M\underline{N}$.

Note that both the block and serial equalization algorithms in this paper need extra complexity for domain transformation. Specifically, $\underline{N}$ BMs and $\underline{N}$ DFTs of size M are required to perform the transform on the demodulated vectors, while $\underline{N}$ BMs and $\underline{N}$ IDFTs of size M are required to perform the inverse transform for the symbol vector estimates. Taking these operations into account, in Table I we summarize the overall complexity of the two proposed time-varying channel equalization algorithms for OSDM in terms of CAs, CMs and CDs. It can be seen that, due to relatively small values of Q, their complexity per vector is approximately only $\mathcal{O}(M\log_2 M)$, which remains on the same order as that of time-invariant channel equalization in (18), and is much lower than the cubic complexity of the direct equalization in [20].

V. CHANNEL ESTIMATION

In Section III, it is assumed that the OSDM receiver has perfect channel knowledge, by which we can obtain the CE-BEM coefficients $\{h_{q,l}\}$ and construct the channel matrices $\overline{\mathbf{C}}$ and $\{\overline{\mathbf{C}}_n\}$ for the block and serial equalizers. However, in practice, doubly-selective channels have to be estimated prior to equalization. To this end, we design an OSDM block structure, as shown in Fig. 5, to facilitate estimation of the CE-BEM coefficients within a single block. Compared to the single-pilot-vector scheme used in [20], the OSDM block here contains U equally spaced pilot vectors, each of which is separated (cyclically) from the data symbol vectors by $2Q$ zero vectors on both sides. As such, the vector size restriction is relaxed from $M \geq L+1$ to $M \geq (L+1)/U$, and thus more flexibility in the OSDM system configuration can be obtained.

[3]We use the term "roughly" because we here do not count the $\mathcal{O}(Q^3 M)$ complexity of the initialization step in Algorithm 3.

Let us denote with $\mathcal{S}_{\rm P} = \{p_0, p_1, \ldots, p_{U-1}\}$ the index set of pilot vectors, where $p_u = Q + u\Delta$ and $\Delta = N/U$ for $u = 0, 1, \ldots, U-1$. Based on (25), it is easy to know that, in this case, the pilot and data symbol vectors can be decoupled. As a result, centered around any vector index $p \in \mathcal{S}_{\rm P}$, there are $2Q+1$ "neat" demodulated vectors $\{\mathbf{x}_{p+q}\}_{q=-Q}^{Q}$, which contain no IVI from data symbol vectors and have signal energy only from the pilot vector $\mathbf{d}_p$. More specifically, we have that, for each $p \in \mathcal{S}_{\rm P}$ and $-Q \leq q \leq Q$,

$$\begin{aligned}\mathbf{x}_{p+q} &= \mathbf{C}_{p+q,p}\mathbf{d}_p + \mathbf{z}_{p+q} \\ &= \mathbf{\Lambda}_M^{(p+q)H}\mathbf{F}_M^H \overline{\mathbf{H}}_{q,p}\mathbf{F}_M \mathbf{\Lambda}_M^p \mathbf{d}_p + \mathbf{z}_{p+q} \end{aligned} \tag{48}$$

where Proposition 4 is used in the second equation. Furthermore, by defining $\overline{\mathbf{x}}_n = \mathbf{F}_M \mathbf{\Lambda}_M^n \mathbf{x}_n$, $\overline{\mathbf{d}}_n = \mathbf{F}_M \mathbf{\Lambda}_M^n \mathbf{d}_n$ and $\overline{\mathbf{z}}_n = \mathbf{F}_M \mathbf{\Lambda}_M^n \mathbf{z}_n$, it can be obtained from (48) that

$$\overline{\mathbf{x}}_{p+q} = \overline{\mathbf{H}}_{q,p}\overline{\mathbf{d}}_p + \overline{\mathbf{z}}_{p+q} = \mathbf{\Pi}_p \mathbf{h}_q + \overline{\mathbf{z}}_{p+q} \tag{49}$$

where

$$\mathbf{\Pi}_p = \mathrm{diag}\{\overline{\mathbf{d}}_p\}\widetilde{\mathbf{F}}_M \mathbf{\Lambda}_{L+1}^p \tag{50}$$

$$\widetilde{\mathbf{F}}_M = \left[\mathbf{1}_{1\times U} \otimes \sqrt{M}\mathbf{F}_M\right]_{:,0:L}. \tag{51}$$

Then, stacking $\mathbf{\Pi}_p$ to form $\mathbf{\Pi}^{(\rm P)} = [\mathbf{\Pi}_{p_0}^T, \mathbf{\Pi}_{p_1}^T, \ldots, \mathbf{\Pi}_{p_{U-1}}^T]^T$, and $\overline{\mathbf{x}}_{p+q}$ to form $\overline{\mathbf{x}}_q^{(\rm P)} = [\overline{\mathbf{x}}_{p_0+q}^T, \overline{\mathbf{x}}_{p_1+q}^T, \ldots, \overline{\mathbf{x}}_{p_{U-1}+q}^T]^T$, we obtain the least-squares estimate of $\mathbf{h}_q$ as

$$\widehat{\mathbf{h}}_q = \mathbf{\Pi}^{(\rm P)\dagger}\overline{\mathbf{x}}_q^{(\rm P)}, q = -Q, -Q+1, \ldots, Q. \tag{52}$$

To further avoid direct matrix inversion in the above equation and thus achieve low-complexity channel estimation, we here select U frequency-shifted Chu sequences [29] to be the pilot vectors, i.e.,

$$\mathbf{d}_p = \mathbf{\Lambda}_M^{pH}\mathbf{b}_M, \qquad p \in \mathcal{S}_{\rm P} \tag{53}$$

where $\mathbf{b}_M$ takes the form

$$[\mathbf{b}_M]_m = e^{j\pi m^2/M}, m = 0, 1, \ldots, M-1. \tag{54}$$

Then, invoking the property that the Chu sequences and their DFTs are constant-modulus [29], we have that $|[\overline{\mathbf{d}}_p]_m| = 1$ for $m = 0, 1, \ldots, M-1$, and thus $\mathbf{\Pi}^{(\rm P)H}\mathbf{\Pi}^{(\rm P)} = MU\mathbf{I}_{L+1}$. Therefore, in this case, the channel estimation in (52) can be rewritten as

$$\widehat{\mathbf{h}}_q = \frac{1}{MU}\sum_{p\in\mathcal{S}_{\rm P}} \mathbf{\Lambda}_{L+1}^{pH}\widetilde{\mathbf{F}}_M^H \mathrm{diag}\left\{\overline{\mathbf{d}}_p^*\right\}\overline{\mathbf{x}}_{p+q}. \tag{55}$$

From (55), it can be seen that matrix inversion is no longer involved and $\widehat{\mathbf{h}}_q$ can be simply computed by performing U IDFT operations of length M. The related complexity is only on the order of $\mathcal{O}(UM\log_2 M)$.

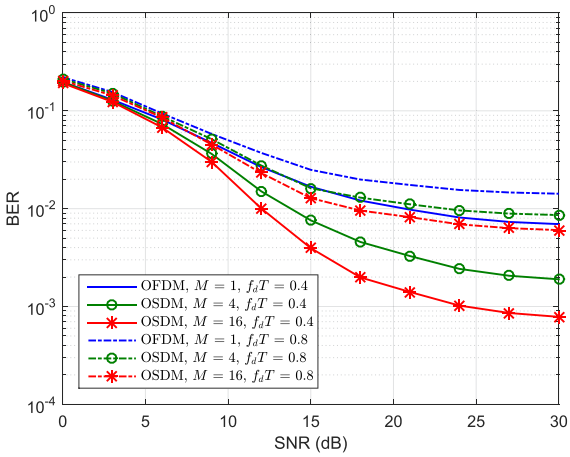

Fig. 6. BER performance of the proposed block OSDM equalization algorithm for different values of M and f_dT.

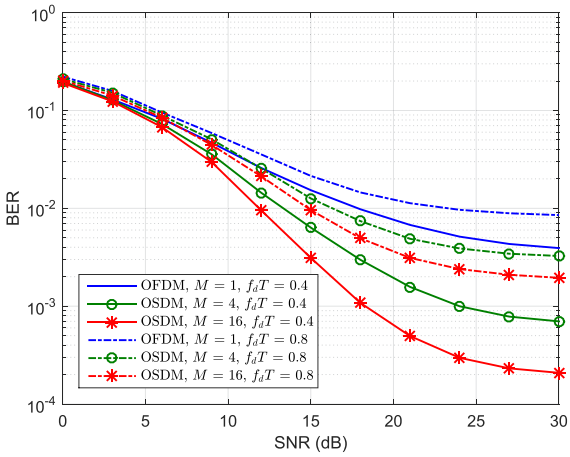

Fig. 7. BER performance of the proposed serial OSDM equalization algorithm for different values of M and f_dT.

VI. Numerical Simulations

In this section, numerical simulation results are provided to illustrate the bit error rate (BER) performances of the proposed low-complexity OSDM equalization algorithms over doubly-selective channels. We here consider a UWA communication scenario, where OSDM blocks are composed of $K = 1024$ quaternary phase-shift keying (QPSK) symbols and have a duration of $T = 256$ ms. The symbol sampling period is thus $T_{\rm s} = T/K = 0.25$ ms. Moreover, to simulate the UWA channel effects, we set the channel memory length to $L = 24$, which corresponds to a multipath delay spread of $\tau_{\max} = LT_{\rm s} = 6$ ms. Independent Rayleigh fading channel taps are assumed with an exponentially decaying power delay profile losing 1.66 dB per tap. Meanwhile, similar to [20], the channel Doppler spread is modeled by a bell-shaped spectrum with bell coefficient equal to 9. The normalized Doppler spread f_dT, where f_d is the maximum Doppler frequency, is changed over the range of $[0, 1]$.

With the above settings, the performance of the proposed algorithms is evaluated in the following four aspects.

1) Comparison With OFDM: Figs. 6 and 7 show the BER performance of the proposed block and serial OSDM equalization algorithms, respectively, with various vector lengths $M = 1$, 4 and 16. For comparison, two normalized Doppler spreads, $f_dT = 0.4$ and 0.8, are considered here. Moreover, at the receiver, we assume perfect knowledge of the time-varying CIR and fix $Q = 2$. The CE-BEM channel coefficients can thus be obtained via (19). Since OSDM reduces to OFDM when $M = 1$, the corresponding curves in the two figures actually correspond to the BER performance of the block and serial OFDM equalization algorithms in [25]. It can be seen that the proposed OSDM equalization algorithms outperform their OFDM counterparts, and lower error floors are achieved as M increases. A similar observation has been reported in [13], [15] over frequency-selective channels, and a detailed theoretical analysis of the diversity order can be found in [13]. An intuitive explanation is based on the precoded-OFDM interpretation of OSDM in Section II-A. Specifically, unlike OFDM where each symbol is modulated independently on one subcarrier, the symbol vectors in OSDM are precoded with $\{\mathbf{F}_M \mathbf{\Lambda}_M^n\}$, and thus the energy of each symbol is distributed over M subcarriers, by which intra-vector frequency diversity can be obtained. However, we should also note that, as f_dT increases, the BER improvement obtained by adjusting M gets smaller. This is because the CE-BEM approximates the doubly-selective channel by ignoring the out-of-band IVI. A larger f_dT leads to a worse CE-BEM approximation and more leakage of the out-of-band IVI, which reduces the frequency diversity gain obtained by increasing M.

Furthermore, by comparing the results in Figs. 6 and 7, it can be seen that serial equalization generally has a better performance than its block equalization counterpart. This is because, given that the CE-BEM enforces a limited Doppler spread Q, block equalization actually uses all $\underline{N}$ demodulated vectors to estimate each symbol vector, while serial equalization excludes the remote demodulated vectors $\{\mathbf{x}_i | |i-n| > Q\}$ (with unmodeled IVI) from participation in estimating $\mathbf{d}_n$.

2) Effects of Channel Doppler Spread: Figs. 8 and 9 illustrate the BER performance of the proposed block and serial OSDM equalization algorithms as a function of the normalized Doppler spread for various Q values. Here, the OSDM vector length is set to $M = 4$ and the signal-to-noise ratio (SNR) is fixed at 20 dB. Again, we assume that perfect channel knowledge is available at the receiver. It is easy to realize that, when $Q = 0$, the IVI effect is ignored and thus time-invariant channel equalization is actually adopted which serves here as a benchmark. As expected, the OSDM system performance improves as Q increases, since the band approximation of the CE-BEM gets enhanced accordingly. However, it is interesting to note that, for some large values of Q, the BER is not monotonically increasing with respect to the Doppler spread. This is because extending the Doppler spread not only worsens the CE-BEM approximation but also improves the Doppler diversity gain. The overall system performance is jointly determined by these two coupling effects. When the Doppler spread is relatively small, the effect of Doppler diversity prevails and the BER decreases slightly. In contrast, as the Doppler spread increases, the effect of the channel modeling error dominates and the BER starts to rise.

3) Impact of Channel Estimation Errors: Fig. 10 compares the BER performance of the proposed block OSDM equalization algorithm with known and estimated channel knowledge.

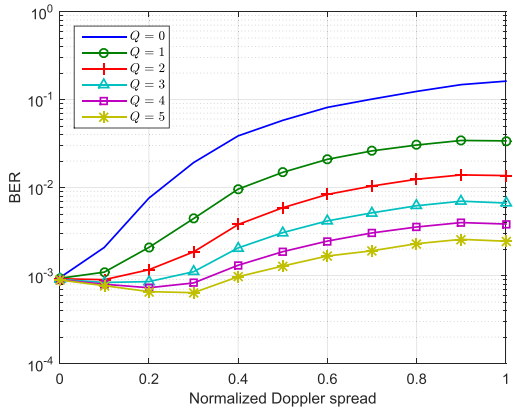

Fig. 8. BER performance of the proposed block OSDM equalization algorithm for different values of Q.

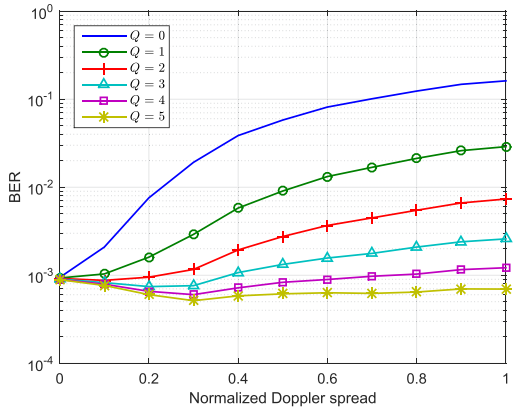

Fig. 9. BER performance of the proposed serial OSDM equalization algorithm for different values of Q.

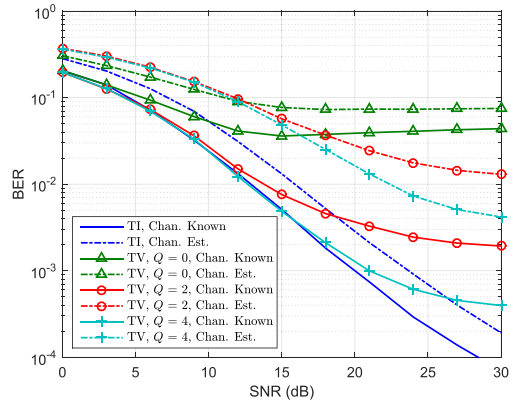

Fig. 10. BER performance comparison of the proposed block OSDM equalization algorithm with known and estimated channel knowledge.

The performance evaluation is carried out over a time-varying (TV) channel with normalized Doppler spread $f_dT = 0.4$, as well as over a time-invariant (TI) channel (with $f_dT = 0$) as a benchmark. Here, the OSDM vector length is fixed to $M = 4$. We select $U = 8$ and thus a total of $MU = 32$ pilot symbols is used for channel estimation. It can be observed that, except for the TI case, there exists an error floor in all TV cases due to the band approximation of the CE-BEM. To reduce the approximation error and improve the BER performance, a simple approach

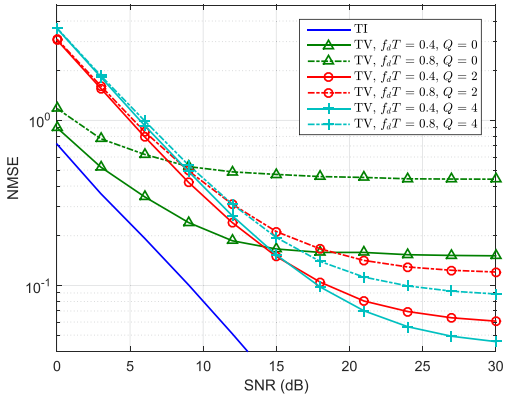

Fig. 11. NMSE performance of the OSDM channel estimation algorithm for different values of f_dT and Q.

is to increase Q when the channel is known. However, this is not always the case when channel estimation is taken into account. The imperfect channel knowledge can negate the performance advantage of configuring $Q > 0$ at low SNR.

To make this clearer, Fig. 11 further presents the channel estimation performance in terms of the normalized mean square error (NMSE). We here use the same OSDM system configurations as those in Fig. 10, and consider two TV cases of $f_dT = 0.4$ and 0.8 (against the benchmark of the TI case). As expected, the NMSE increases with f_dT. However, we cannot draw the simple conclusion here that the NMSE decreases with Q. Actually, it can be seen that, although a larger Q introduces additional CE-BEM coefficients for TV channel modeling, at low SNR, their estimates are unreliable and thus lead to a higher NMSE.

Finally, it may be worth mentioning that, with Q fixed, the CE-BEM approximation can also be improved by using a receiver window design similar to that in [30]. However, an investigation of this topic goes beyond the scope of this paper.

4) Comparison With D-OSDM Equalization [20]: Since the D-OSDM equalization in [20] is performed on the entire data block and thus can be categorized as block equalization, we compare it with the block OSDM equalization proposed in this paper. Also for fairness, given that the D-OSDM receiver supports only the single-pilot-vector channel estimation scheme [20], we select $U = 1$ and use a longer vector length $M = 32$ here to make sure $MU > L$. Meanwhile, we fix the SNR to 20 dB and the channel normalized Doppler spread to $f_dT = 0.4$. It can be seen in Fig. 12 that, although producing the same BER at $Q = 0$, the proposed block equalization improves its performance more slowly than the D-OSDM equalization as Q increases. And its inferior performance becomes evident at large values of Q, especially when the channel is perfectly known at the receiver. The reason for this phenomenon is that, unlike the D-OSDM equalization which makes full use of all N demodulated vectors, the proposed block equalization algorithm uses only the truncated block in (31) comprising $\underline{N} = N - 2Q$ demodulated vectors. Anyway, the performance gap between these two equalization algorithms is quite narrow when channel estimation is taken into account. And, more importantly, the computational complexity of the proposed block equalization algorithm is only

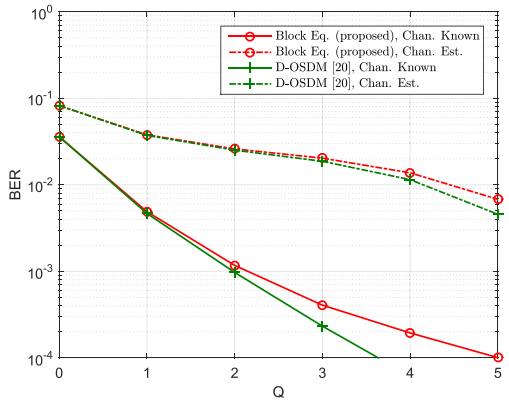

Fig. 12. BER performance comparison between the proposed block OSDM equalization algorithm and the D-OSDM equalization algorithm in [20].

about 0.02% of that of its D-OSDM equalization counterpart when $Q = 5$.

VII. Conclusion

OSDM is a generalized modulation scheme which can merge OFDM and SC-FDE in a unified framework and offer more flexibility in system design. However, OSDM suffers from IVI over doubly-selective channels. In this paper, low-complexity block and serial equalization algorithms have been proposed to counteract its effect. Unlike the direct equalization in (31) and (42) of cubic complexity, these proposed algorithms exploit the cyclically block-banded structure of the composite channel matrix (Proposition 4), and are performed in a transformed domain. Then, by using block LDL^H factorization (Algorithm 1) and block iterative matrix inversion (Algorithm 3), the equalization complexities are significantly reduced to about $\mathcal{O}(M\log_2 M)$ per symbol vector. These OSDM equalization algorithms are based on the CE-BEM, and can be regarded as an extension of the corresponding algorithms for OFDM in [25]. Moreover, to facilitate their practical implementation, a CE-BEM channel estimation method has been designed for OSDM systems (Fig. 5 and (55)), which uses frequency-shifted Chu sequences as pilots to ease the computation. Numerical simulations are finally provided to confirm the validity of our algorithms, and to further examine the impact of the vector length, Doppler spread and channel estimation error on the BER performance. The results suggest that, equipped with these low-complexity equalization algorithms, OSDM could be potentially considered for future high-rate wireless communications over doubly-selective channels.

Appendix A
Proof of Proposition 1 and (8)

Proposition 1 is actually based on the general Cooley-Tukey algorithm [31], which decomposes the calculation of an DFT of size $K = MN$ into M smaller DFTs of size N. Let $\mathbf{x} = [x_0, x_1, \ldots, x_{K-1}]^T$ be the input sequence, $\mathbf{y} = [y_0, y_1, \ldots, y_{K-1}]^T$ be the corresponding unitary DFT output sequence, and $W_K = e^{-j2\pi/K}$ denote the primitive Kth root of unity. Then, at any index $k = mN + n$ for $m = 0, 1, \ldots, M-1$ and $n = 0, 1, \ldots, N-1$, the unitary DFT output sample can be derived as [31]

$$\begin{aligned} y_{mN+n} &= \frac{1}{\sqrt{K}} \sum_{l=0}^{K-1} x_l W_K^{l(mN+n)} \\ &= \frac{1}{\sqrt{K}} \sum_{p=0}^{M-1} \left[\left(\sum_{q=0}^{N-1} x_{qM+p} W_N^{qn} \right) W_K^{pn} \right] W_M^{pm}. \end{aligned} \tag{56}$$

By collecting all K DFT output samples, the above DFT factorization can be described in matrix-vector form as

$$\mathbf{y} = \mathbf{F}_K \mathbf{x} = \mathbf{P}_{N,M} \left(\mathbf{I}_N \otimes \mathbf{F}_M \right) \mathbf{\Lambda} \left(\mathbf{F}_N \otimes \mathbf{I}_M \right) \mathbf{x} \tag{57}$$

from which Proposition 1 is proved.

We then use the DFT matrix factorization identity in Proposition 1 to derive the precoded-OFDM interpretation of OSDM. Specifically, by plugging (3) and (5) into the left-hand side of (8), it can be obtained that

$$\begin{aligned} \mathbf{F}_K \mathbf{s} &= \left[\mathbf{P}_{N,M} \left(\mathbf{I}_N \otimes \mathbf{F}_M \right) \mathbf{\Lambda} \left(\mathbf{F}_N \otimes \mathbf{I}_M \right) \right] \left[\left(\mathbf{F}_N^H \otimes \mathbf{I}_M \right) \mathbf{d} \right] \\ &= \mathbf{P}_{N,M} \left(\mathbf{I}_N \otimes \mathbf{F}_M \right) \mathbf{\Lambda} \mathbf{d} \end{aligned} \tag{58}$$

where we have used the Kronecker product property, i.e.,

$$\left(\mathbf{A}_1 \otimes \mathbf{B}_1 \right) \left(\mathbf{A}_2 \otimes \mathbf{B}_2 \right) = \left(\mathbf{A}_1 \mathbf{A}_2 \right) \otimes \left(\mathbf{B}_1 \mathbf{B}_2 \right) \tag{59}$$

in the third line. Now, from (58), we can easily arrive at the right-hand side of (8), which concludes the proof.

Appendix B
Proof of Proposition 3

From (11) and (20), we have

$$\mathbf{C} = \sum_{q=-Q}^{Q} \mathbf{\Gamma}_q \mathbf{G}_q \tag{60}$$

where

$$\mathbf{\Gamma}_q = \left(\mathbf{F}_N \otimes \mathbf{I}_M \right) \widetilde{\mathbf{\Gamma}}_K^q \left(\mathbf{F}_N^H \otimes \mathbf{I}_M \right) \tag{61}$$

$$\mathbf{G}_q = \left(\mathbf{F}_N \otimes \mathbf{I}_M \right) \widetilde{\mathbf{G}}_q \left(\mathbf{F}_N^H \otimes \mathbf{I}_M \right). \tag{62}$$

Let us first focus on (62). Since $\widetilde{\mathbf{G}}_q$ is a circulant matrix, which has a similar structure as $\widetilde{\mathbf{C}}$ in (9), based on Proposition 2, (22), (23) and (24) can be readily obtained. We then proceed to (61). Since $\widetilde{\mathbf{\Gamma}}_K^q = \widetilde{\mathbf{\Gamma}}_N^q \otimes \mathbf{\Lambda}_M^{-q}$, by using the Kronecker product property in (59), it can be derived that

$$\begin{aligned} \mathbf{\Gamma}_q &= (\mathbf{F}_N \otimes \mathbf{I}_M)(\widetilde{\mathbf{\Gamma}}_N^q \otimes \mathbf{\Lambda}_M^{-q})(\mathbf{F}_N^H \otimes \mathbf{I}_M) \\ &= (\mathbf{F}_N \widetilde{\mathbf{\Gamma}}_N^q \mathbf{F}_N^H) \otimes \mathbf{\Lambda}_M^{-q}. \end{aligned} \tag{63}$$

Furthermore, by exploiting the well-known property that any $N \times N$ circulant matrix $\mathbf{A}_N$ can be diagonalized by the DFT matrix $\mathbf{F}_N$ as [32]

$$\mathbf{A}_N = \mathbf{F}_N \operatorname{diag}\left(\sqrt{N} \mathbf{F}_N^H \mathbf{a} \right) \mathbf{F}_N^H, \tag{64}$$

where $\mathbf{a}$ is the first column of $\mathbf{A}_N$, we obtain that $\mathbf{F}_N \widetilde{\mathbf{\Gamma}}_N^q \mathbf{F}_N^H$ in (63) is a circulant matrix with its first column equal to

$$\frac{1}{\sqrt{N}} \mathbf{F}_N \left[1, e^{j\frac{2\pi}{N}q}, \ldots, e^{j\frac{2\pi}{N}q(N-1)} \right]^T = \mathbf{e}_N(q). \tag{65}$$

Or in other words, we have

$$\mathbf{F}_N \widetilde{\mathbf{\Gamma}}_N^q \mathbf{F}_N^H = \mathbf{J}_N^q. \tag{66}$$

Finally, by plugging (66) and (63) into (60), we arrive at (21), from which (25) can be readily obtained. This concludes the proof of Proposition 3.

Appendix C
Proof of Proposition 4

We establish the block structure of $\mathbf{C}$ in (21) in three cases, respectively. First, if $|n-n'| \leq Q$, the block $\mathbf{C}_{n,n'}$ is located in the main block band of $\mathbf{C}$. It can be seen from Fig. 2(a) and (21) that we have

$$\mathbf{C}_{n,n'} = \mathbf{\Lambda}_M^{(n-n')H} \mathbf{H}_{n-n',n'}. \tag{67}$$

By plugging (23) into (67), it is obtained that

$$\begin{aligned}\mathbf{C}_{n,n'} &= \mathbf{\Lambda}_M^{(n-n')H} \left(\mathbf{\Lambda}_M^{n'H} \mathbf{F}_M^H \overline{\mathbf{H}}_{n-n',n'} \mathbf{F}_M \mathbf{\Lambda}_M^{n'} \right) \\ &= \mathbf{\Lambda}_M^{nH} \mathbf{F}_M^H \overline{\mathbf{H}}_{n-n',n'} \mathbf{F}_M \mathbf{\Lambda}_M^{n'}\end{aligned} \tag{68}$$

and thus $\overline{\mathbf{C}}_{n,n'} = \overline{\mathbf{H}}_{n-n',n'}$ in this case.

In the second case, if $N-Q \leq n-n' \leq N-1$, the block $\mathbf{C}_{n,n'}$ resides in the bottom-left corner of $\mathbf{C}$. We can derive accordingly that

$$\begin{aligned}\mathbf{C}_{n,n'} &= \mathbf{\Lambda}_M^{(n-n'-N)H} \mathbf{H}_{n-n'-N,n'} \\ &= \mathbf{\Lambda}_M^{(n-n'-N)H} \left(\mathbf{\Lambda}_M^{n'H} \mathbf{F}_M^H \overline{\mathbf{H}}_{n-n'-N,n'} \mathbf{F}_M \mathbf{\Lambda}_M^{n'} \right) \\ &= \mathbf{\Lambda}_M^{nH} \left(\widetilde{\mathbf{\Gamma}}_M^{-1} \mathbf{F}_M^H \right) \overline{\mathbf{H}}_{n-n'-N,n'} \mathbf{F}_M \mathbf{\Lambda}_M^{n'} \\ &= \mathbf{\Lambda}_M^{nH} \left(\mathbf{F}_M^H \mathbf{J}_M^{-1} \right) \overline{\mathbf{H}}_{n-n'-N,n'} \mathbf{F}_M \mathbf{\Lambda}_M^{n'}\end{aligned} \tag{69}$$

where we have used (66) in the last line. From (69), we arrive at $\overline{\mathbf{C}}_{n,n'} = \mathbf{J}_M^{-1} \overline{\mathbf{H}}_{n-n'-N,n'}$.

Finally, in the case that $1-N \leq n-n' \leq Q-N$, the block $\mathbf{C}_{n,n'}$ resides in the top-right corner of $\mathbf{C}$. Its derivation is similar to that in the second case, due to which we omit the details and complete our proof.

Appendix D
Derivations of Algorithm 3

1) Update the matrix $\underline{\overline{\mathbf{R}}}_n$: Since $\widetilde{\mathbf{\Theta}}_n$ and $\widetilde{\mathbf{U}}_n$ are blocks making up the last M columns of $\underline{\overline{\mathbf{R}}}_n$, we have

$$\begin{aligned}\begin{bmatrix} \widetilde{\mathbf{\Theta}}_n \\ \widetilde{\mathbf{U}}_n \end{bmatrix} &= \left[\underline{\overline{\mathbf{C}}}_n \underline{\overline{\mathbf{C}}}_n^H + \sigma^2 \mathbf{I}_{M(2Q+1)} \right]_{:,2QM:2QM+M-1} \\ &= \begin{bmatrix} \overline{\mathbb{C}}_{n-Q,n} & & \\ \vdots & \ddots & \\ \overline{\mathbb{C}}_{n+Q,n} & \cdots & \overline{\mathbb{C}}_{n+Q,n+2Q} \end{bmatrix} \begin{bmatrix} \overline{\mathbb{C}}_{n+Q,n}^H \\ \vdots \\ \overline{\mathbb{C}}_{n+Q,n+2Q}^H \end{bmatrix} \\ &\quad + \begin{bmatrix} \mathbf{0}_{2QM \times M} \\ \sigma^2 \mathbf{I}_M \end{bmatrix}\end{aligned} \tag{70}$$

from which the update equations of $\underline{\overline{\mathbf{R}}}_n$ in lines 4–7 of Algorithm 3 can be obtained.

2) Compute the matrix $\mathbf{\Sigma}_n^{-1}$: Substituing (46) and (47) into $\underline{\overline{\mathbf{R}}}_{n-1} \underline{\overline{\mathbf{R}}}_{n-1}^{-1} = \mathbf{I}_{M(2Q+1)}$, we can obtain that

$$\mathbf{\Theta}_{n-1} \mathbf{\Phi}_{n-1}^H + \mathbf{\Sigma}_n \mathbf{\Xi}_{n-1} = \mathbf{I}_{2QM} \tag{71}$$

$$\mathbf{\Theta}_{n-1} \mathbf{V}_{n-1} + \mathbf{\Sigma}_n \mathbf{\Phi}_{n-1} = \mathbf{0}_{2QM \times M}. \tag{72}$$

From (71), it yields that $\mathbf{\Sigma}_n^{-1} = \mathbf{\Sigma}_n^{-1} \mathbf{\Theta}_{n-1} \mathbf{\Phi}_{n-1}^H + \mathbf{\Xi}_{n-1}$. Then, given that $\mathbf{\Sigma}_n^{-1} \mathbf{\Theta}_{n-1} = -\mathbf{\Phi}_{n-1} \mathbf{V}_{n-1}^{-1}$, which is derived from (72), we have that $\mathbf{\Sigma}_n^{-1}$ is the Schur complement of $\mathbf{V}_{n-1}$ in $\underline{\overline{\mathbf{R}}}_{n-1}^{-1}$, i.e., the equation in line 9 of Algorithm 3.

3) Update the matrix $\underline{\overline{\mathbf{R}}}_n^{-1}$: Similarly, by substituing (46) and (47) into $\underline{\overline{\mathbf{R}}}_n \underline{\overline{\mathbf{R}}}_n^{-1} = \mathbf{I}_{M(2Q+1)}$, it can be obtained that

$$\mathbf{\Sigma}_n \widetilde{\mathbf{\Phi}}_n + \widetilde{\mathbf{\Theta}}_n \widetilde{\mathbf{V}}_n = \mathbf{0}_{2QM \times M} \tag{73}$$

$$\mathbf{\Sigma}_n \widetilde{\mathbf{\Xi}}_n + \widetilde{\mathbf{\Theta}}_n \widetilde{\mathbf{\Phi}}_n^H = \mathbf{I}_{2QM} \tag{74}$$

$$\widetilde{\mathbf{\Theta}}_n^H \widetilde{\mathbf{\Phi}}_n + \widetilde{\mathbf{U}}_n \widetilde{\mathbf{V}}_n = \mathbf{I}_{M \times M}. \tag{75}$$

Here, from (73), we have $\widetilde{\mathbf{\Phi}}_n = -\mathbf{\Sigma}_n^{-1} \widetilde{\mathbf{\Theta}}_n \widetilde{\mathbf{V}}_n = \mathbf{\Omega}_n \widetilde{\mathbf{V}}_n$, i.e., the equation in line 13 of Algorithm 3. Then, plugging it into (75), we arrive at the equation of updating $\widetilde{\mathbf{V}}_n$ in line 12 of Algorithm 3. Also, based on $\widetilde{\mathbf{\Phi}}_n = \mathbf{\Omega}_n \widetilde{\mathbf{V}}_n$ and (74), we obtain the equation of updating $\widetilde{\mathbf{\Xi}}_n$ in line 14 of Algorithm 3.

References

[1] Z. Wang and G. B. Giannakis, "Wireless multicarrier communications: Where Fourier meets Shannon," *IEEE Signal Process. Mag.*, vol. 17, no. 3, pp. 29–48, May 2000.

[2] Y. Rahmatallah and S. Mohan, "Peak-to-average power ratio reduction in OFDM systems: A survey and taxonomy," *IEEE Commun. Surveys Tuts.*, vol. 15, no. 4, pp. 1567–1592, Oct. 2013.

[3] D. Falconer, S. Ariyavisitakul, A. Benyamin-Seeyar, and B. Eidson, "Frequency domain equalization for single-carrier broadband wireless systems," *IEEE Commun. Mag.*, vol. 40, no. 4, pp. 58–66, Apr. 2002.

[4] F. Pancaldi, G. Vitetta, R. Kalbasi, N. Al-Dhahir, M. Uysal, and H. Mheidat, "Single-carrier frequency domain equalization," *IEEE Commun. Mag.*, vol. 25, no. 5, pp. 37–56, Sep. 2008.

[5] N. Suehiro, C. Han, T. Imoto, and N. Kuroyanagi, "An information transmission method using Kronecker product," in *Proc. IASTED Int. Conf. Commun. Syst. Netw.*, Sep. 2002, pp. 206–209.

[6] N. Suehiro, C. Han, and T. Imoto, "Very efficient wireless frequency usage based on pseudo-coherent addition of multipath signals using Kronecker product with rows of DFT matrix," in *Proc. Int. Symp. Inf. Theory*, Jun. 2003, pp. 385–385.

[7] X.-G. Xia, "Precoded and vector OFDM robust to channel spectral nulls and with reduced cyclic prefix length in single transmit antenna systems," *IEEE Trans. Commun.*, vol. 49, no. 8, pp. 1363–1374, Aug. 2001.

[8] C. Han, T. Hashimoto, and N. Suehiro, "Constellation-rotated vector OFDM and its performance analysis over Rayleigh fading channels," *IEEE Trans. Commun.*, vol. 58, no. 3, pp. 828–838, Mar. 2010.

[9] H. Zhang, X.-G. Xia, Q. Zhang, and W. Zhu, "Precoded OFDM with adaptive vector channel allocation for scalable video transmission over frequency-selective fading channels," *IEEE Trans. Mobile Comput.*, vol. 1, no. 2, pp. 132–142, Apr. 2002.

[10] H. Zhang, X.-G. Xia, L. J. Cimini, and P. C. Ching, "Synchronization techniques and guard-band-configuration scheme for single-antenna vector-OFDM systems," *IEEE Trans. Wireless Commun.*, vol. 4, no. 5, pp. 2454–2464, Sep. 2005.

[11] H. Zhang and X.-G. Xia, "Iterative decoding and demodulation for single-antenna vector OFDM systems," *IEEE Trans. Veh. Technol.*, vol. 55, no. 4, pp. 1447–1454, Jul. 2006.

[12] P. Cheng, M. Tao, Y. Xiao, and W. Zhang, "V-OFDM: On performance limits over multi-path Rayleigh fading channels," *IEEE Trans. Commun.*, vol. 59, no. 7, pp. 1878–1892, Jul. 2011.

[13] Y. Li, I. Ngebani, X.-G. Xia, and A. Host-Madsen, "On performance of vector OFDM with linear receivers," *IEEE Trans. Signal Process.*, vol. 60, no. 10, pp. 5268–5280, Oct. 2012.

[14] J. Han and G. Leus, "Space-time and space-frequency block coded vector OFDM modulation," *IEEE Commun. Lett.*, vol. 21, no. 1, pp. 204–207, Jan. 2017.
[15] J. Han, S. P. Chepuri, Q. Zhang, and G. Leus, "Iterative per-vector equalization for orthogonal signal-division multiplexing over time-varying underwater acoustic channels," *IEEE J. Ocean. Eng.*, Jan. 2018, to be published, doi: 10.1109/JOE.2017.2787898.
[16] I. Ngebani, Y. Li, X.-G. Xia, S. Haider, A. Huang, and M. Zhao, "Analysis and compensation of phase noise in vector OFDM systems," *IEEE Trans. Signal Process.*, vol. 62, no. 23, pp. 6143–6157, Dec. 2014.
[17] I. Ngebani, Y. Li, X. G. Xia, and M. Zhao, "EM-based phase noise estimation in vector OFDM systems using linear MMSE receivers," *IEEE Trans. Veh. Technol.*, vol. 65, no. 1, pp. 110–122, Jan. 2016.
[18] T. Ebihara and K. Mizutani, "Underwater acoustic communication with an orthogonal signal division multiplexing scheme in doubly spread channels," *IEEE J. Ocean. Eng.*, vol. 39, no. 1, pp. 47–58, Jan. 2014.
[19] J. Han, W. Shi, and G. Leus, "Space-frequency coded orthogonal signal-division multiplexing over underwater acoustic channels," *J. Acoust. Soc. Amer.*, vol. 141, no. 6, pp. EL513–EL518, Jun. 2017.
[20] T. Ebihara and G. Leus, "Doppler-resilient orthogonal signal-division multiplexing for underwater acoustic communication," *IEEE J. Ocean. Eng.*, vol. 41, no. 2, pp. 408–427, Apr. 2016.
[21] M. Stojanovic and J. Preisig, "Underwater acoustic communication channels: Propagation models and statistical characterization," *IEEE Commun. Mag.*, vol. 47, no. 1, pp. 84–89, Jan. 2009.
[22] F. Qu, Z. Wang, L. Yang, and Z. Wu, "A journey toward modeling and resolving Doppler in underwater acoustic communications," *IEEE Commun. Mag.*, vol. 54, no. 2, pp. 49–55, Feb. 2016.
[23] B. Li, S. Zhou, M. Stojanovic, L. Freitag, and P. Willett, "Multicarrier communication over underwater acoustic channels with nonuniform Doppler shifts," *IEEE J. Ocean. Eng.*, vol. 33, no. 2, pp. 198–209, Apr. 2008.
[24] P. Schniter, "Low-complexity equalization of OFDM in doubly selective channels," *IEEE Trans. Signal Process.*, vol. 52, no. 4, pp. 1002–1011, Apr. 2004.
[25] L. Rugini, P. Banelli, and G. Leus, "Simple equalization of time-varying channels for OFDM," *IEEE Commun. Lett.*, vol. 9, no. 7, pp. 619–621, Jul. 2005.
[26] F. Hlawatsch and G. Matz, *Wireless Communications Over Rapidly Time-Varying Channels*. New York, NY, USA: Academic, 2011, pp. 42–43.
[27] I. Barhumi, G. Leus, and M. Moonen, "Equalization for OFDM over doubly selective channels," *IEEE Trans. Signal Process.*, vol. 54, no. 4, pp. 1445–1458, Apr. 2006.
[28] X. Cai and G. B. Giannakis, "Bounding performance and suppressing intercarrier interference in wireless mobile OFDM," *IEEE Trans. Commun.*, vol. 51, no. 12, pp. 2047–2056, Dec. 2003.
[29] D. Chu, "Polyphase codes with good periodic correlation properties," *IEEE Trans. Inf. Theory*, vol. 18, no. 4, pp. 531–532, Jul. 1972.
[30] L. Rugini, P. Banelli, and G. Leus, "Low-complexity banded equalizers for OFDM systems in Doppler spread channels," *EURASIP J. Appl. Signal Process.*, vol. 2006, pp. 1–13, Aug. 2006, Art. no. 67404.
[31] P. Duhamel and M. Vetterli, "Fast Fourier transforms: A tutorial review and a state of the art," *Signal Process.*, vol. 19, no. 4, pp. 259–299, Apr. 1990.
[32] G. H. Golub and C. F. Van Loan, *Matrix Computations*, 4th ed. Baltimore, MD, USA: Johns Hopkins Univ. Press, 2013.

Jing Han (M'10) received the B.Sc. degree in electrical engineering, and the M.Sc. and Ph.D. degrees in signal and information processing, all from Northwestern Polytechnical University, Xi'an, China, in 2000, 2003, and 2008, respectively. He is currently an Associate Professor with the School of Marine Science and Technology, Northwestern Polytechnical University. From June 2015 to June 2016, he was a Visiting Researcher with the Faculty of Electrical Engineering, Mathematics and Computer Science, Delft University of Technology, Delft, The Netherlands. His research interests include wireless communications, statistical signal processing, and particularly their applications to underwater acoustic systems. He is an Associate Editor for the *EURASIP Signal Processing*.

Lingling Zhang (M'17) received the M.Sc. and Ph.D. degrees in information and communication engineering from Northwestern Polytechnical University, Xi'an, China, in 2011 and 2017, respectively. She is currently an Assistant Researcher with the School of Marine Science and Technology, Northwestern Polytechnical University. From October 2012 to April 2014, she was a Visiting Researcher with the Department of Electrical Engineering, University of Virginia, Charlottesville, VA, USA. Her research interests include wireless communications, statistical signal processing, and particularly their applications to underwater acoustic systems.

Qunfei Zhang (M'03) received the B.Sc. degree in electronic engineering, the M.S. degree in signal and information processing, both from Northwestern Polytechnical University, Xi'an, China, in 1990 and 1993, respectively, and the Ph.D. degree in signal and information processing from Xidian University, Xi'an, China, in 2003. He is currently a Professor with the School of Marine Science and Technology, Northwestern Polytechnical University. His research interests include spectral estimation, array signal processing, and underwater communications and networking.

Geert Leus (M'01–SM'05–F'12) received the M.Sc. and Ph.D. degrees in electrical engineering from the KU Leuven, Leuven, Belgium, in June 1996 and May 2000, respectively. He is currently an "Antoni van Leeuwenhoek" Full Professor with the Faculty of Electrical Engineering, Mathematics and Computer Science, Delft University of Technology, Delft, The Netherlands. His research interest includes the broad area of signal processing, with a specific focus on wireless communications, array processing, sensor networks, and graph signal processing. He was a member-at-large of the Board of Governors of the IEEE Signal Processing Society, the Chair of the IEEE Signal Processing for Communications and Networking Technical Committee, and the Editor-in-Chief for the *EURASIP Journal on Advances in Signal Processing*. He was also on the editorial boards of the IEEE TRANSACTIONS ON SIGNAL PROCESSING, the IEEE TRANSACTIONS ON WIRELESS COMMUNICATIONS, the IEEE SIGNAL PROCESSING LETTERS, and the *EURASIP Journal on Advances in Signal Processing*. He is currently an Associate Editor for *Foundations and Trends in Signal Processing* and the Editor-in-Chief for the *EURASIP Signal Processing*. He is the recipient of the 2002 IEEE Signal Processing Society Young Author Best Paper Award and the 2005 IEEE Signal Processing Society Best Paper Award. He is a Fellow of EURASIP.